Adeno-associated virus Rep proteins antagonize phosphatase PP1 to counteract KAP1 repression of the latent viral genome

Short title: ***KAP1 repression of the latent AAV genome***

Sarah Smith-Moore[a], Stuart J. Neil[a], Cornel Fraefel[b], R. Michael Linden[a], Mathieu Bollen[c], Helen M. Rowe[d], and Els Henckaerts[a,1]

Author Affiliation: [a]Department of Infectious Diseases, School of Immunology and Microbial Sciences, King's College London, Great Maze Pond, London, SE1 9RT, UK. [b]Institute of Virology, University of Zurich, Rämistrasse 71, 8006 Zurich, Switzerland. [c]KU Leuven Department of Cellular and Molecular Medicine, University of Leuven, B-3000 Leuven, Belgium. [d]Centre for Medical Molecular Virology, Division of Infection and Immunity, University College London, 90 Gower Street, London WC1E 6BT.

[1]Corresponding author: Els Henckaerts, Department of Infectious Diseases, School of Immunology and Microbial Sciences, King's College London, Great Maze Pond, London, SE1 9RT, UK; telephone number: +44 (0)207 848 9620; email address: els.henckaerts@kcl.ac.uk

Classification: Biological Sciences: Microbiology

Key words: adeno-associated virus, latency, KAP1, Rep, PP1, NIPP1

Abstract

Adeno-associated virus (AAV) is a small human *dependovirus* whose low immunogenicity and capacity for long term persistence have led to its widespread use as vector for gene therapy. Despite great recent successes in AAV-based gene therapy, further improvements in vector technology may be hindered by an inadequate understanding of various aspects of basic AAV biology. AAV is unique in that its replication is largely dependent on a helper virus and cellular factors, and in the absence of coinfection, wild type AAV establishes latency through mechanisms that are not yet fully understood. Challenging the currently held model for AAV latency, we show here that the corepressor Krüppel-associated box domain-associated protein 1 (KAP1) binds the latent AAV2 genome at the *rep* ORF, leading to trimethylation of AAV2-associated histone 3 lysine 9, and that the inactivation of KAP1 repression is necessary for AAV2 reactivation and replication. We identify a new viral mechanism for the counteraction of KAP1, in which interference with the KAP1 phosphatase protein phosphatase 1 (PP1) by the AAV2 Rep proteins mediates enhanced phosphorylation of KAP1-S824, and thus relief from KAP1 repression. Furthermore, we show that this phenomenon involves recruitment of the NIPP1 (nuclear inhibitor of PP1)-PP1α holoenzyme to KAP1 in a manner dependent upon the NIPP1 FHA domain, identifying NIPP1 as a novel interaction partner for KAP1 and shedding light on the mechanism through which PP1 regulates cellular KAP1 activity.

Significance statement

In recent years, adeno-associated virus (AAV) has attracted considerable attention as a result of its success as a gene therapy vector. However, several aspects of its biology remain elusive. Given that AAV vectors mimic the latent phase of the viral life cycle, defining the mechanisms involved in the regulation of AAV latency is of particular importance. Our studies demonstrate, for the first time, that epigenetic processes are involved in the regulation of viral latency and reveal novel virus-host interactions and helper functions that are aimed at counteracting the epigenetic repression of the viral

genome during the lytic phase of the viral life cycle. These observations will inform the design of future AAV vector technologies.

BODY

Introduction

Adeno-associated virus serotype 2 (AAV2) is a small, single-stranded DNA (ssDNA) parvovirus that has evolved a unique biphasic life cycle in which replication is dependent on both cellular host factors and coinfection by a helper virus such as adenovirus (Ad5) or herpesvirus (HSV-1) (1). Unable to replicate autonomously, infection by AAV2 alone leads to the establishment of latency either through long term episomal persistence (2), or through preferential integration of the viral genome into specific sites in the human genome (3–5). The current model for AAV2 latency states that the viral genome is silenced through simultaneous binding of the viral p5 promoter by the AAV2 master regulator Rep and the cellular transcription factors YY1 and MLTF, and that the induction of AAV2 gene expression upon helper virus coinfection occurs through interactions between these factors and the helper factor Ad5 E1A or HSV-1 ICP0 (6–8). Despite the widely accepted view that latent AAV2 is silenced exclusively through the binding of Rep and YY1 to p5, evidence that the viral genome assumes a chromatinized configuration shortly after infection (9, 10) suggests a role for epigenetic modification in the establishment of latency and/or transcriptional regulation. The epigenetic landscape of AAV remains unknown however.

Recent years have seen a rapidly expanding interest in the AAV field as a result of its widespread use as a vector for gene therapy. Despite great recent successes in AAV-based gene therapy (11–16), further improvements may be hindered by an inadequate understanding of various aspects of basic AAV biology. Given that AAV vectors likely mimic the latent phase of the viral life cycle, defining the mechanisms involved in the regulation of AAV latency is of particular importance

for the future design and safety of improved vectors. In this study, we sought to gain insight into the regulation of AAV latency by using a screening approach known as BioID (17) to identify novel interaction partners for the AAV2 replication (Rep) proteins. BioID exploits the fusion of the promiscuous biotin ligase BirA* to a bait protein in order to trigger proximity-dependent biotinylation of neighboring proteins, thus allowing for the identification of a much broader scope of protein associations than achievable with conventional affinity purification.

Screens were performed using each of the four related Rep isoforms – Rep78, Rep68, Rep52, and Rep40 – which together orchestrate every aspect of the viral life cycle. The large Rep proteins (Rep78/68) consist of an origin-binding domain (OBD) containing site-specific DNA binding and endonuclease activity (18) and an ATPase domain with helicase activity (19), and are necessary for viral replication, integration, and transcriptional regulation (20–22). The small Rep proteins (Rep52/40) share only the ATPase domain, and are involved mostly in viral packaging and transcriptional regulation (23, 24). In addition, Rep52 and Rep78 share a C-terminal zinc finger (ZNF) domain implicated in several protein interactions (25, 26). Our BioID screen identified the transcriptional corepressor Krüppel-associated box domain-associated protein 1 (KAP1/TRIM28/ TIF1-β) as an interaction partner of the Rep proteins and led to the discovery that Rep78 and Rep52 interact with a protein complex containing KAP1, protein phosphatase 1 (PP1), and nuclear inhibitor of PP1 (NIPP1) in order to counteract KAP1-mediated repression of the latent viral genome.

Results

The latent AAV2 genome is repressed through KAP1 recruitment to the *rep* ORF and subsequent histone methylation.

For the BioID screen, BirA* was fused to the N-terminus of each of the four Rep isoforms, and the BirA*-Rep fusion proteins were expressed in 293T cells in the presence of free biotin. Biotinylated proteins were affinity purified 48h after transfection and analyzed by LC-MS/MS. Identified in

lysates from each of the four screens was the corepressor KAP1, which acts to form transcriptionally repressive heterochromatin through the recruitment of chromatin-modifying proteins such as the histone methyltransferase SETDB1 and the NuRD histone deacetylase complex containing CHD3 (27, 28). Peptides identified for KAP1 are shown in Table S1. Several known interaction partners of the Rep proteins were also identified by BioID (Table S1), lending support to the quality and coherence of our results. The well documented function of KAP1 as a mediator of heterochromatin (29, 30) combined with a growing body of evidence demonstrating a role for KAP1 in the regulation of viral elements (31–34) led us to focus our efforts on this candidate. With the exception of Rep68, the physical interaction between each of the Rep proteins and KAP1 was confirmed using biotinylation and immunoprecipitation assays (Fig. S1). Given that Rep40 represents the only shared domain between the Rep proteins, these results suggest that the central Rep ATPase domain is sufficient to mediate a Rep-KAP1 interaction but that the C-terminal ZNF domain of Rep78 is necessary to stabilize this interaction in the presence of an N-terminal OBD.

To explore the possible significance of the Rep-KAP1 interaction in the AAV life cycle, we next performed viral replication experiments in cells depleted for KAP1. 293T cells were transduced with lentiviral vectors expressing either a shRNA targeting the 3' UTR of KAP1 (shKAP1), or the corresponding empty vector (shEMPTY). 48h later, cells were infected with Ad5 alone, AAV2 alone, or coinfected with Ad5 and AAV2 in order to initiate productive replication. Viral replication and transcription were analyzed approximately 42h after infection, or when cells displayed optimal cytopathic effect. AAV2 replication was undetectable in either KAP1-depleted or control cells in the absence of Ad5, however this was expected as AAV2 is known to be dependent on several helper factors to initiate replication. In the context of coinfection however, a 5-6-fold enhancement in AAV2 genome replication, transcription, and protein expression was observed in KAP1-depleted cells as compared to controls (Fig. 1 *A* and *B*, Fig. S2), Importantly, complementation of KAP1-depleted

cells with exogenous *KAP1* restored baseline levels of AAV2 replication and protein expression (Fig. 1*C*, Fig. S2).

We next asked if KAP1 could be repressing AAV2 through its recruitment to the viral genome and subsequent formation of heterochromatin. We performed KAP1-specific chromatin immunoprecipitation (ChIP) on 293T cells 2 days after infection with AAV2 alone and analyzed the purified chromatin by qPCR using primers specific for various regions of the AAV2 genome. *GAPDH* was used as a negative control, and two zinc finger genes, *ZNF180* and *ZNF274*, as positive controls (35). KAP1 binding was detected across *rep*, particularly at the 5' and middle regions (Fig. 1*D,* Fig. S3), corresponding with the genomic location of the AAV2 p19 promoter. Binding was accordingly lost in KAP1-depleted cells, confirming the observed signal was KAP1-dependent. To determine the functional significance of this binding, we also performed ChIP-qPCR for H3K9me3, a known marker for KAP1-mediated repression. H3K9me3 was enriched across the AAV2 genome (Fig. 1*E,* Fig. S3), spreading downstream from KAP1 binding sites in *rep*. Furthermore, this enrichment appeared to be KAP1-dependent as H3K9 trimethylation was lost in KAP1-depleted cells at a ratio similar to what was observed for controls *ZNF180* and *ZNF274*. Importantly, depletion of CHD3 and SETDB1, two members of the KAP1 repressive complex (27, 28), independently and cooperatively led to an enhancement in AAV2 replication and protein expression (Fig. 1 *F, G,* and *H*). Taken together, these data strongly suggest that KAP1 represses AAV2 through the binding of AAV2 *rep* and the subsequent recruitment of histone and chromatin modifying proteins, which then act together to methylate AAV2-associated H3K9.

Inactivation of KAP1 repression through phosphorylation of serine 824 is necessary to support AAV2 transcriptional activation and lytic replication.

Upon DNA damage, ATM-dependent phosphorylation of KAP1 at serine 824 (p-KAP1-S824) results in release of the repressive complex, relaxation of heterochromatin, and relief of transcriptional

repression (36, 37). We questioned whether AAV2 replication was associated with KAP1-S824 phosphorylation, which would suggest a requirement for the inactivation of KAP1 corepressor activity. We first explored this possibility by monitoring levels of phosphorylated KAP1-S824 in cells infected with increasing concentrations of either AAV2 or recombinant AAV2 (rAAV2) in the presence of Ad5. rAAV2 is comprised of only the viral inverted terminal repeats (ITRs) flanking a GFP transgene cassette, and as such is replication defective. However, the ITRs are known to recruit components of the Mre11/Rad50/NBS1 (MRN) complex – the principal mediator of ATM activation – and could potentially trigger KAP1-S824 phosphorylation (38). We therefore used rAAV2 to control for the input of these structures.

A clear dose-dependent increase in KAP1-S824 phosphorylation was observed in 293T cells coinfected with Ad5 and increasing concentrations of AAV2 (Fig. 2*A*). This was not observed in the presence of rAAV2, which is replication defective and therefore additionally requires Rep and Cap *in trans* for replication (Fig. 2*A*), suggesting that active AAV2 replication is necessary to trigger KAP1-S824 phosphorylation and not simply the viral structure represented by rAAV2. In addition, H3K9me3-specific ChIP performed in cells coinfected with AAV2 and Ad5 revealed a complete loss of H3K9 trimethylation on lytic AAV2 genomes, indicating that release of the KAP1 repressive complex is necessary to support lytic replication (Fig. 2*B*). The observation that AAV2 replication levels are reduced in cells overexpressing wild-type KAP1 ($KAP1^{WT}$) (Fig. 2*C*) and enhanced with overexpression of the dominant negative phospho-mimetic KAP1-S824D mutant ($KAP1^{S824D}$) (Fig. 2*D*) further supports a functional role for KAP1-S824 phosphorylation in AAV2 replication. Furthermore, KAP1-depleted cells complemented with $KAP1^{S824D}$ supported enhanced levels of AAV2 replication and protein expression, which were comparable to those observed in KAP1-depleted cells, whereas complementation with the phospho-ablatant mutant $KAP1^{S824A}$ restored replication and protein expression to baseline levels (Fig. 2 *E* and *F*).

To determine whether KAP1-S824 phosphorylation constitutes a viral reactivation switch, we looked at the effect of KAP1-S824 phosphorylation on basal expression levels from the three AAV promoters in the absence of helper virus coinfection. AAV transcription during latency is virtually undetectable, and furthermore it has been well established that a helper factor such as Ad5 E1A is essential for activation of the p5 promoter (6). To observe measurable effects on basal AAV2 transcription, these experiments were therefore necessarily performed in 293T cells, which are transformed with AdV E1/E2 and can thus support extremely low levels of AAV transcription without helper virus coinfection. Cells depleted for KAP1 and reconstituted with $KAP1^{WT}$, $KAP1^{S824D}$, or $KAP1^{S824A}$ were infected with AAV2 alone and harvested 14h post-infection for transcriptional analysis. Both KAP1-depleted cells and cells reconstituted with $KAP1^{S824D}$ supported 2- to 6-fold greater levels of basal transcription from the three AAV2 promoters, while complementation with $KAP1^{WT}$ and $KAP1^{S824A}$ restored transcription to negligible levels (Fig. 2*G*).

Rep52 and Rep78 mediate phosphorylation of KAP1-S824 through interactions with the protein phosphatase PP1.

We next performed a time course of lytic replication to determine if phosphorylation of KAP1-S824 could be related to the onset of Rep expression. Substantially elevated levels of p-KAP1-S824 were apparent 18h after infection with Ad5 and AAV2, correlating well with the onset of Rep expression and leading us to ask if the Rep proteins might be directly modulating KAP1 activity (Fig. 3*A*). To address this, cells expressing various mutants of the Rep proteins were monitored for p-KAP1-S824 levels. The large Rep proteins possess endonuclease activity shown to trigger DNA damage (25, 39), and all four Rep proteins share a helicase domain with the potential to also disrupt DNA. In order to minimize the possibility of DDR-dependent induction of p-KAP1-S824 via ATM, endonuclease mutants (Y156F) of Rep68 and Rep78, and catalytic ATPase mutants (K340H) of all four Rep proteins were used (40, 41). Substantially elevated levels of p-KAP1-S824 were apparent

196 in the presence of both Rep52 and Rep78, independently from either endonuclease or ATPase
197 activity (Fig. 3*B*). Basal levels of p-KAP1-S824 were also visible with Rep40 and Rep68 but were
198 3- to 6-fold lower than for Rep52 and Rep78. These data suggest that the Rep proteins, in particular
199 Rep52 and Rep78, actively mediate phosphorylation of KAP1-S824 via an unknown pathway,
200 independently from their ability to cause DNA damage. This idea was further supported by
201 transfection and infection experiments performed in the presence of an ATM inhibitor (ATMi),
202 which demonstrated that ATM activation is not necessary for the observed Rep-mediated
203 phosphorylation of KAP1-S824 (Fig. S4). Given that Rep52 and Rep78 share a C-terminal ZNF
204 domain not present in Rep40 or Rep68, we suspected this region might also be important for the
205 phosphorylation of KAP1-S824. Expression of a series of C-terminal truncation mutants, in which
206 the Rep52/Rep78 ZNF domain was progressively removed (Fig. S5), completely abrogated
207 phosphorylation of KAP1-S824 while having no effect on the Rep-KAP1 interaction (Fig. S5),
208 suggesting that the Rep proteins act through an intermediary protein(s).

209 Potential cellular factors that could be interacting with Rep to control the phosphorylation
210 state of KAP1-S824 include protein phosphatase 1 (PP1) and its specific regulators. Upon
211 completion of DNA repair, basal levels of p-KAP1-S824 are restored through the combined
212 activities of PP1α/β and protein phosphatase 4 (42, 43). Several regulatory subunits of PP1 were
213 identified as interaction partners for Rep alongside KAP1 in our original BioID screen, leading us
214 to hypothesize that the Rep proteins could be interfering with this pathway and antagonizing PP1
215 activity. Co-IP experiments in cells expressing Rep52 and GFP-tagged PP1-α, -β, or -γ indicated a
216 physical interaction between Rep52, PP1α, and PP1γ (Fig. 3*C*). Furthermore, AAV2 lytic
217 replication and transcription were enhanced with depletion of PP1α but not PP1β (Fig. 3 *D, E,* and
218 *F*), supporting observations from the co-IP as well as a role for PP1 antagonism in the AAV life
219 cycle. Interestingly, this effect was most pronounced at early time points indicating that PP1 might
220 act predominantly during early infection events, such as transcriptional activation.

Using the conserved PP1 consensus binding sequence [KR][X_{0-1}][VI]{P}[FW] (44) as our guideline, we identified one putative non-canonical binding site in the Rep ATPase domain (372KMVIW376), partially overlapping with the Walker B motif (Fig. S6). Co-IP experiments using FLAG-tagged PP1α confirmed a physical interaction between Rep52 and PP1α (Fig. 3*G*). Mutation of the first lysine in the putative binding site (K372A) did not affect this interaction however (Fig. 3*G*), indicating this region may not represent a true PP1 binding site. Alternatively, it is possible that this region acts together with the Rep ZNF domain to bind PP1. Interestingly however, the K372A mutation completely abrogated Rep-mediated phosphorylation of KAP1-S824 (Fig. 3*H*) without affecting the ability of Rep to regulate the AAV2 p5 promoter (45) or interact with KAP1 (Fig. S6). There is precedence to indicate that a functional interaction between PP1 and its regulatory subunits is based on multiple points of interaction, only one of which necessarily consists of the conserved binding site. Furthermore it has been demonstrated that mutation of only one interaction site may be sufficient to abolish the regulation of PP1 while being insufficient to abolish the physical association between PP1 and its regulatory component (46, 47). It is therefore possible that the mutation of additional yet unidentified interaction sites in Rep would be necessary to disrupt Rep-PP1 binding, while mutation of only the PP1 binding site is sufficient to abolish regulation of PP1 by Rep.

The Rep proteins interfere with the formation of a KAP1-NIPP1-PP1 complex to inhibit KAP1-S824 dephosphorylation by PP1.

The free PP1 catalytic subunit has exceptionally broad substrate specificity. PP1 activity is therefore regulated through its interactions with numerous PP1-interacting-proteins (PIPs), which can inhibit PP1 or act as substrate specifiers (48). To further define a potential mechanism for the above observations, we next looked at the nuclear inhibitor of PP1 (NIPP1/PPP1R8), a major regulator of PP1 that was identified alongside KAP1 in our BioID screen. NIPP1 contains three

functional domains: (1) an N-terminal Forkhead Associated (FHA) protein interaction domain, (2) a central PP1-binding domain containing the consensus PP1-binding motif, and (3) a multifunctional C-terminal domain that binds RNA, has endoribonuclease activity, and inhibits PP1 activity via an unknown mechanism (46, 49, 50). Cross-linked GFP-trap experiments in cells expressing Rep52 with various NIPP1 mutants (Fig. 4*A*) fused to eGFP revealed that KAP1 and Rep are recruited to NIPP1 via the N-terminal FHA domain, forming a complex with the NIPP1-PP1α holoenzyme (Fig. 4*B*). PP1α has previously been shown to form a constitutive unit with KAP1 at certain promoters (42). Our results suggest however that, in this instance, the interaction between KAP1 and PP1 is mediated through NIPP1. Recruitment was dependent upon the NIPP1 FHA domain, which binds hyperphosphorylated proteins through a dipeptide motif consisting of phospho-threonines followed by a proline. Although no function has yet been attributed to it, one such motif exists at threonine 541 of KAP1 suggesting that it may be directly recruited to NIPP1 via the FHA domain. Levels of p-KAP1-S824 were elevated in cells overexpressing NIPP1-WT compared to cells expressing the PP1-binding mutant NIPP1-RATA, supporting a role for the inhibition of PP1 by NIPP1 in KAP1 phosphorylation (Fig. 4 *C* and *D*). Surprisingly, p-KAP1-S824 levels were also elevated in the presence of NIPP1-FHAm. It is possible that the residual binding observed between KAP1 and NIPP1-FHAm (Fig. 4*B*) is sufficient to support the regulation of phosphorylation. Alternatively, overexpression of NIPP1-FHAm may act to constitutively inhibit the nuclear pool of PP1. In addition, NIPP1-WT and NIPP1-FHAm, but not NIPP1-RATA, enhanced Rep-mediated phosphorylation of KAP1-S824 (Fig. 4 *E* and *F*), supporting the idea that this pathway is exploited by Rep to maintain enhanced levels of p-KAP1-S824 during infection.

To further explore the role for Rep in this pathway, we performed cross-linked GFP-trap experiments in cells expressing NIPP1-WT-eGFP with either wild type Rep52, or the phosphorylation-deficient Rep52-K372A (Fig. 4*G*). Interestingly, recruitment of KAP1 to NIPP1 appeared to be independent of Rep52 entirely, while abundance of PP1α in the complex was

significantly decreased in the presence of Rep52, but not Rep52-K372A. The loss of PP1α was associated with increased p-KAP1-S824 and a concomitant loss of SETDB1, supporting the hypothesis that Rep52 mediates phosphorylation of KAP1-S824 through PP1 interference in order to counteract KAP1 repression. Furthermore, as loss of PP1α from the complex was observed with Rep52 but not Rep52-K372A, these results suggest that the K372A mutation may in fact interfere with the Rep-PP1 interaction in the context of endogenous PP1 even though we did not observe an effect with overexpressed FLAG-PP1α (Fig. 3*G*).

Targeting of KAP1 as a novel helper function for AAV2 replication.

Given that basal levels of Rep expression during latency are not sufficient to counteract KAP1 and that depletion of KAP1 alone is not sufficient to trigger AAV2 transcription and replication, we hypothesized that AAV2 helper viruses might act as a biological switch necessary to allow for the upregulation of *rep* expression prior to the onset of KAP1 phosphorylation. KAP1 protein levels were significantly depleted in 293T and HeLa cells infected with increasing concentrations of Ad5 and were restored in the presence of 5μM of the proteasome inhibitor MG132 (Fig. S7). Interestingly, Ad5 E1B55K has been shown to interfere with KAP1 SUMOylation during early infection (51), presenting the possibility that hypoSUMOylated KAP1 may be targeted by the cell for proteosomal degradation. Similar results were also observed for HSV-1, another AAV helper virus (Fig. S7), suggesting that KAP1 targeting may represent an unknown helper function for AAV2 replication necessary to release the viral genome from its latent state.

Discussion

Significant breakthroughs in AAV vector design have previously been derived from an enhanced understanding of basic AAV biology. There are still many aspects of the AAV life cycle that remain elusive however. Of particular relevance to AAV vectors, whose biology may mimic that

296 of latent viral genomes, the nature and contribution of epigenetic marks to the genome organization
297 and temporal gene regulation of wild type AAV is not yet known. In the present study, we employed
298 a BioID strategy to screen for novel interaction partners of the AAV2 Rep proteins in an effort to
299 elucidate the mechanisms involved in the establishment of and release from AAV2 latency. This
300 approach led to the discovery that the transcriptional corepressor KAP1 interacts with three of the
301 four Rep proteins and is recruited to the latent AAV2 genome, where it mediates transcriptional
302 repression through the formation of heterochromatin.

303 Our findings bear interesting parallels with observations made for the regulation of both
304 KSHV and CMV latency by KAP1. Recruitment of KAP1 to the CMV genome leads to H3K9me3
305 deposition across various lytic genes, while latency-associated genes remain free from repressive
306 marks (32). Similarly, latency associated nuclear antigen (LANA)-mediated recruitment of KAP1 to
307 the KSHV genome is essential for the shutdown of lytic gene expression during early stages of
308 infection (52). Here, we observed KAP1-dependent deposition of H3K9me3 across the latent AAV2
309 genome, spreading downstream from KAP1 recruitment sites near the p19 promoter in *rep* in a
310 manner consistent with the mechanism of long-range heterochromatin spreading shown to establish
311 KAP1-mediated repression of KRAB-ZFP clusters (53). Interestingly, no enrichment for KAP1 or
312 H3K9me3 was detected at the p5 promoter, a region whose transactivating activity is necessary for
313 initiation from all three viral promoters. It will be interesting to determine whether this region is
314 protected from repressive marks in order to ensure rapid and dynamic regulation of p5 upon
315 reactivation.

316 In agreement with a role for KAP1 as a repressor of latent AAV2, both KAP1 depletion and
317 expression of a repression-deficient phosphomimetic KAP1-S824D mutant resulted in enhanced lytic
318 replication, transcription, and protein expression in cells coinfected with AAV2 and Ad5. This effect
319 was not observed in cells infected with AAV2 alone however, reflecting the dependency of AAV2
320 on various helper factors to initiate replication and suggesting that KAP1 repression provides a

second layer of regulation, the antagonism of which is necessary but not sufficient for reactivation. Similar observations were made for both KSHV and CMV. KSHV replication was enhanced, but not triggered, by KAP1 depletion, both in the context of induced KRta expression and hypoxia-induced KSHV reactivation (31, 54). Similarly, TNFα-mediated NF-κB induction was necessary for the full reactivation of CMV upon KAP1 depletion (32). It is well established that reactivation of AAV2 is dependent upon interactions between helper factors such as Ad5 E1A and cellular factors YY1 and MLTF bound to the p5 promoter region. Our observation that levels of basal AAV2 transcription in latently infected 293T cells were enhanced in cells either depleted for KAP1 or reconstituted with KAP1-S824D however strongly indicates that KAP1 binding additionally serves to silence the viral genome through histone methylation, even while the p5 promoter may be minimally activated by low levels of E1A. We therefore propose that AAV2 reactivation is dependent upon the removal of repressive H3K9me3 from the viral genome in order to render it transcriptionally competent and allow for E1A-mediated activation of p5, and thus, transactivation of all three viral promoters.

It is also interesting to note that KSHV, CMV, and AAV2 are episomal viruses with the ability to modulate KAP1 activity, which are clearly capable of replication without the need for KAP1 depletion, suggesting the intriguing possibility that these viruses have domesticated KAP1 repression to their advantage. It is possible for example that heterochromatinization allows latent episomes to better evade immune recognition, or that it may prevent deleterious recombination events and/or genome degradation. Upon reactivation, KSHV directly mediates phosphorylation of KAP1 via its viral kinase vPk (31), and, although it is has not yet been established which CMV protein is responsible, phosphorylation of KAP1-S824 was only ever observed in cells that were also positive for CMV IE antigens (32). Here, we show that AAV2 Rep52 and Rep78 mediate the inactivation of KAP1 repression by inhibiting its dephosphorylation by the phosphatase PP1α. Rep expression reduced the abundance of PP1α from a complex comprised of KAP1, SETDB1, PP1α, and NIPP1, and this was dependent upon the presence of an intact putative PP1-binding site in Rep, suggesting

346 that Rep52 achieves enhanced phosphorylation of KAP1-S824 by sequestering PP1 from the
347 complex.

348 Although we have shown that Rep can mediate the phosphorylation of KAP1 independently
349 from ATM activation, this does not exclude a role for the activation of effectors of the DDR in the
350 context of a productive infection. In fact, the nature of the mechanism outlined above presupposes
351 an initial trigger for KAP1 phosphorylation, and both helper virus and productive AAV2 infections
352 are known to trigger robust activation of DDR proteins (55, 56). Taken together, these data suggest
353 a two-part mechanism in which helper factors or the DDR upon viral infection trigger the initial
354 phosphorylation of KAP1, a signal then potentiated through Rep-mediated antagonism of PP1 during
355 lytic replication. We envision that the inactive NIPP1-PP1 holoenzyme forms a constitutive
356 regulatory unit with KAP1, effectively serving to tether inactive PP1 to KAP1 for rapid regulation
357 (Fig. S8). NIPP1 does not systematically inhibit PP1 activity however. Rather, inhibition is dependent
358 upon interactions between PP1 bound to the central domain of NIPP1 and the inhibitory C-terminal
359 domain of NIPP1, which additionally has RNA binding and endoribonuclease activity (46, 47). This
360 interaction can be interrupted through the simultaneous phosphorylation of tyrosine 335 in the C-
361 terminal domain and binding of RNA, effectively activating the PP1-NIPP1 holoenzyme (46). Upon
362 initiation of a DDR, when KAP1 is rapidly phosphorylated, NIPP1 inhibition of PP1 may be
363 inactivated through RNA-binding and phosphorylation of the C-terminal region of NIPP1 by the
364 DDR-responsive tyrosine kinase Lyn (46), allowing PP1 to rapidly restore basal levels of p-KAP1-
365 S824. The role of the Rep proteins might then be to sequester PP1, or compete for binding, in order
366 to sustain high levels of p-KAP1-S824 and support lytic infection (Fig. 5, Fig. S8).

367 This work demonstrates not only the first example of PP1 targeting by a parvovirus, but also
368 the first example of PP1 targeting for the purpose of regulating KAP1 activity. It will be interesting
369 to determine whether this mechanism might extend to other members of the parvovirus family, or if
370 known viral targets of KAP1 such as KSHV and CMV might also manipulate this pathway to achieve

relief from KAP1 repression. PP1 has previously been shown to form a constitutive unit with KAP1 at the *p21* promoter, where it is thought to set a basal transcription rate as well as to rapidly restore KAP1 corepressor function after ATM activation by regulating KAP1-S824 phosphorylation (42). There is no evidence for free cellular pools of PP1 however. Rather, PP1 constitutes the catalytic unit of a large array of multisubunit holoenzymes, which regulate and target PP1 activity to prevent uncontrolled protein dephosphorylation and cell death (48). It has yet to be determined what PP1 interacting protein (PIP) is responsible for regulating PP1 activity towards KAP1. Our finding that KAP1, PP1, and NIPP1 exist as a complex sheds light on this question and suggests that PP1 may be targeted to KAP1 via the NIPP1 FHA domain where it is then dynamically regulated by NIPP1 to maintain homeostatic levels of phosphorylated KAP1-S824.

This work further presents the first evidence that AAV2 latency is regulated in part through the epigenetic modification of its genome, challenging the long-standing model for AAV latency whereby the viral genome is silenced exclusively through binding of the p5 promoter by cellular factors YY1 and MLTF, and the Rep proteins (6, 57). The findings presented here have additional relevance for gene therapy, as our data highlight the possibility that current production helper plasmids may lack helper genes that may be critical for navigating host responses. Understanding the epigenetic control of AAV may also shed light on the intriguing and unexplained resistance of AAV gene therapy vectors to host shut off, and will undoubtedly contribute to understanding the consequences of integrating wild type and recombinant viruses. In addition, the recent controversial discovery of AAV2 sequences in human liver tumors (58) has caused some to call into question the safety of rAAV vectors and has highlighted the need to further explore AAV2 regulation of latency. These findings may thus provide key insights into the impact and contribution of AAV2 latency on the development of human diseases.

Methods

Cell lines and viruses

293T human embryonic kidney cells and HeLa human cervical epithelial cells were obtained from the American Tissue Culture Collection (ATCC). Cells were cultured in Dulbecco's modified Eagle's (DMEM) (Invitrogen) supplemented with 10% fetal bovine serum (FBS) (Invitrogen) plus 1% Pen/Strep (Sigma) and were tested for mycoplasma once per month.

AAV2 and human adenovirus type 5 (Ad5) were produced and purified as previously described (59).

BioID Screening

Ten 10cm dishes of 293T cells per BirA*-Rep construct were transfected using 6µg DNA and 50µl PEI in 500µl serum-free (SF) medium per dish. 6h post-transfection, the medium was replaced with fresh DMEM + 10% FBS, and D-Biotin (Life Technologies) was added to a final concentration of 100µM. 48h post-transfection, cells were harvested for LC-MS/MS analysis as previously described (17). Mass spectrometry was performed by the KCL Proteomics Facility at Denmark Hill.

Immunoprecipitation

293T cells were transfected in a 6-well format with 200ng of Rep-expressing constructs, and 250ng of FLAG-PP1α or FAG-GFP using 8µl PEI in 80µl serum free (SF) medium. 48h after transfection, cells were lysed in RIPA buffer, and lysates were incubated with 2µg anti-FLAG (Sigma, F7425) for 1.5h on a rotator at 4°C. 40µl of protein G agarose beads (Pierce) were added and incubated a further 3h. Beads were washed 4 times in RIPA buffer, and proteins were eluted from beads by boiling at 95^{o}C for 10 minutes in 60µl 2X Laemmli buffer.

Cross-linking Immunoprecipitation

293T cells were transfected in a 6-well format with 200ng of Rep-expressing constructs, and 750ng of FLAG-GFP, FLAG-KAP1, or GFP-NIPP1 using 8µl PEI in 80µl SF medium. 48 hours after transfection cells were fixed in 350µl 0.05% formaldehyde for 10 minutes at 37°C and then quenched in 350µl 0.125M glycine, pH 7, for 5 minutes at room temperature before being lysed in 500µl cross-linking IP buffer (150mM NaCl, 10mM HEPES pH 7, 6mM $MgCl_2$, 2mM DTT, 10% glycerol, 1X protease inhibitors, 200uM sodium orthovanadate) on ice for 10 minutes. Lysates were subjected to three 10-second cycles of sonication (Branson Sonifier 250), output ~2, and clarified at 1000 x g for 10 minutes at 4°C. 40ml protein G agarose beads (Pierce) per sample were incubated with 2µg FLAG antibody (Sigma, F7425) for 1.5h on a rotator at 4°C before being added to the cell lysates and incubated a further 3-4 hours. Beads were harvested and washed 4 times in RIPA buffer, and cross-links were reversed in 25µl reverse cross-link buffer (10mM EDTA, 5mM DTT, 1% SDS) at 65°C for 45 minutes. Proteins were eluted from beads by adding 3µl of 2X Laemmli SDS buffer and boiling at 95ºC for 10 minutes. For GFP-trap experiments, 293T cells were transfected with 800ng of Rep- and/or NIPP1-expressing constructs. 24h after transfection, cells were harvested as described above, and cell lysates were incubated with 30µl NHS-activated sepharose (GEhealthcare) covalently linked to GFP nanobodies. Beads were harvested as described above.

Infections

For KAP1 depletion, 293T cells were transduced with a lentiviral vector expressing either a hairpin targeting the 3'UTR of KAP1, or the corresponding empty vector, 48h before infection with AAV2/Ad5. Cells were infected at ~80% confluency with 10 IU/cell of AAV2 unless stated otherwise in ~2/5 the normal well volume. 2h after AAV2 infection, Ad5 was added at an MOI of 2 PFU/cell, and medium was replaced with fresh DMEM + 10% FBS 1h after Ad5 infection. Cells were harvested for qPCR, RT-qPCR, or western blot ~42h after infection, or when they displayed optimal cytopathic effect (CPE). Optimal CPE is defined by cells that display a rounded and enlarged

phenotype, as opposed to the normal "star-shaped" morphology of HEK293T cells, and which are beginning to detach but still appear bright and healthy. Cells that had completely lifted by the time of harvest were deemed too advanced in the infection cycle and were excluded from analysis.

ChIP-qPCR

Cells were cross-linked in their medium in 1% formaldehyde (10' at room temperature) and quenched with 0.125M glycine (5' at room temperature) before being lysed in 1mL/1x10^8 cells lysis buffer (50mM Tris-HCl, pH 8, 10mM EDTA, 1% SDS, 1x protease inhibitors) for 10' on ice. Lysates were sonicated to obtain 200- to 500-bp fragments (15 x 30" cycles with 90" intervals, output ~2). 10ml of lysates were used to assess sonication efficiency by reverse cross-linking for 15' at 95°C and then incubating with RNAse A for 30' at 37 degrees. DNA was extracted and visualized on a 1.5% agarose gel. The remaining lysates were clarified at 13,000 rpm for 10' at 4 degrees. The equivalent of 2x10^6 cells was diluted 25-fold in RIPA buffer (50mM Tris pH8, 150mM NaCl, 2mM EDTA, pH 8, 1% NP-40, 0.5% sodium deoxycholate, 0.1% SDS, 1x protease inhibitors) and pre-cleared with 80ml protein G agarose beads (pre-blocked in 0.1mg/mL BSA for 30') for 2h on a rotator at 4°C. For the immunoprecipitation, antibodies were added to lysates and incubated with antibody for 1h on a rotator at 4°C (5mg IgG [Abcam; ab37415], 4mg H3K9me3 [Abcam; ab8893], 1mg KAP1 [Abcam; ab10483]), before adding 80ml pre-blocked beads and incubating overnight as above. Beads were harvested and washed 4 times in RIPA buffer, 4 times in high salt wash (20mM Tris-HCl, pH 8, 1mM EDTA, 500mM NaCl, 0.5% NP-40, 1x protease inhibitors), 4 times in TE buffer (10mM Tris-HCl, pH8, 1mM EDTA), and eluted in 160ml elution buffer (100mM $HaHCO_3$, 1% SDS) for 15' at 30°C. Cross-links were reversed by adding NaCl to a final concentration of 0.2M and incubating overnight at 67°C. Eluates were then incubated with 2ml RNase A (10mg/mL) and 2ml proteinase K (20mg/mL) at 45 degrees for 1h. DNA was extracted using a PCR purification kit (Qiagen) and analyzed by qPCR using primers specific for GAPDH, ZNF180, ZNF274, or various regions of the

AAV2 genome. Purified chromatin was diluted 10-fold and quantified by real-time PCR using the SYBR Green JumpStart Taq ReadyMix for QPCR (Sigma-Aldrich) using an ABI PRISM system (Applied Biosystems). Primer sequences are listed in the Extended Data Table 2. CT values for "10% input" were adjusted by subtracting 3.322 cycles to correct for the 10-fold dilution factor (https://www.thermofisher.com/uk/en/home/life-science/epigenetics-noncoding-rna-research/chromatin-remodeling/chromatin-immunoprecipitation-chip/chip-analysis.html). Percent input was then calculated as follows: 100 x 2^-(CT of adjusted 10% input - CT of ChIP-ed DNA). Percent input for each antibody was then normalized to values for IgG to calculate final fold enrichment.

Acknowledgements We thank M. Bardelli, G. Berger, R. Galão, T.Foster, and S. Pickering for their technical assistance. We thank C. Swanson for his insightful comments and support. This work was supported by UK MRC grants 1001764 to R.M.L., and MR/N022890/1 to E. H.

Author Contributions S.S conceived and performed experiments, and wrote the manuscript. S.N., M.B., and H.M.R. provided reagents, expertise, and feedback. C.F. provided reagents. R.M.L. provided expertise and feedback, and secured funding. E.H. conceived experiments, wrote the manuscript, and secured funding.

References

1. Henckaerts E, Linden RM (2010) Adeno-associated virus: a key to the human genome? *Futur Virol* 5(5):555–574.
2. Schnepp BC, Jensen RL, Chen CL, Johnson PR, Clark KR (2005) Characterization of adeno-associated virus genomes isolated from human tissues. *J Virol* 79(23):14793–14803.
3. Petri K, et al. (2015) Presence of a trs-Like Motif Promotes Rep-Mediated Wild-Type

Adeno-Associated Virus Type 2 Integration. *J Virol* 89(14):7428–32.

4. Janovitz T, et al. (2013) High-throughput sequencing reveals principles of adeno-associated virus serotype 2 integration. *J Virol* 87(15):8559–68.

5. Huser D, Gogol-Doring A, Chen W, Heilbronn R (2014) Adeno-Associated Virus Type 2 Wild-Type and Vector-Mediated Genomic Integration Profiles of Human Diploid Fibroblasts Analyzed by Third-Generation PacBio DNA Sequencing. *J Virol* 88(19):11253–11263.

6. Chang LS, Shi Y, Shenk T (1989) Adeno-associated virus P5 promoter contains an adenovirus E1A-inducible element and a binding site for the major late transcription factor. *J Virol* 63(8):3479–3488.

7. Geoffroy, Epstein, Toublanc, Moullier (2004) Herpes simplex virus type 1 ICP0 protein mediates activation of adeno-associated virus type 2 rep …. *J Virol*. doi:10.1128/JVI.78.20.10977.

8. Shi Y, Seto E, Chang LS, Shenk T (1991) Transcriptional repression by YY1, a human GLI-Kruppel-related protein, and relief of repression by adenovirus E1A protein. *Cell* 67(2):377–388.

9. Marcus-Sekura CJ, Carter BJ (1983) Chromatin-like structure of adeno-associated virus DNA in infected cells. *J Virol* 48(1):79–87.

10. Penaud-Budloo M, et al. (2008) Adeno-associated virus vector genomes persist as episomal chromatin in primate muscle. *J Virol* 82(16):7875–7885.

11. Nathwani AC, et al. (2014) Long-Term Safety and Efficacy of Factor IX Gene Therapy in Hemophilia B. *N Engl J Med* 371(21):1994–2004.

12. Bainbridge JWB, et al. (2015) Long-Term Effect of Gene Therapy on Leber's Congenital Amaurosis. *N Engl J Med* 372(20):1887–97.

13. Bennet J, et al. (2016) Safety and durability of effect of contralateral-eye administration of

AAV2 gene therapy in patients with childhood-onset blindness caused by RPE65 mutations: a follow-on phase 1 trial. *Lancet*.

14. Mendell JR, et al. (2017) Single-Dose Gene-Replacement Therapy for Spinal Muscular Atrophy. *N Engl J Med* 377(18):1713–1722.

15. George LA, et al. (2017) Hemophilia B Gene Therapy with a High-Specific-Activity Factor IX Variant. *N Engl J Med* 377(23):2215–2227.

16. Perry D, et al. (2017) AAV5–Factor VIII Gene Transfer in Severe Hemophilia A. 1–12.

17. Roux KJ, Kim DI, Raida M, Burke B (2012) A promiscuous biotin ligase fusion protein identifies proximal and interacting proteins in mammalian cells. *J Cell Biol* 196(6):801–810.

18. Im DS, Muzyczka N (1990) The AAV origin Bonding protein Rep 68 is an ATP-dependent site-specific endonuclease with DNA helicase activity. *Cell* 61:447–457.

19. Im DS, Muzyczka N (1992) Partial purification of adeno-associated virus Rep78, Rep52, and Rep40 and their biochemical characterization. *J Virol* 66(2):1119–1128.

20. Chejanovsky N, Carter BJ (1989) Mutagenesis of an AUG codon in the adeno-associated virus rep gene: Effects on viral DNA replication. *Virology* 173(1):120–128.

21. Surovsky R, et al. (1997) Adeno-associated virus Rep proteins target DNA sequences to a unique locus in the human genome. *J Virol* 71(10):7951–7959.

22. Pereira DJ, Muzyczka N (1997) The cellular transcription factor SP1 and an unknown cellular protein are required to mediate Rep protein activation of the adeno-associated virus p19 promoter. *J Virol* 71(3):1747–1756.

23. King JA, Dubielzig R, Grimm D, Kleinschmidt JA (2001) DNA helicase-mediated packaging of adeno-associated virus type 2 genomes into preformed capsids. *EMBO J* 20(12):3282–3291.

24. Kyöstiö SR, et al. (1994) Analysis of adeno-associated virus (AAV) wild-type and mutant

Rep proteins for their abilities to negatively regulate AAV p5 and p19 mRNA levels. *J Virol* 68(5):2947–57.

25. Berthet C, Raj K, Saudan P, Beard P (2005) How adeno-associated virus Rep78 protein arrests cells completely in S phase. *Proc Natl Acad Sci U S A* 102(38):13634–13639.

26. Di Pasquale G, Stacey SN (1998) Adeno-associated virus Rep78 protein interacts with protein kinase A and its homolog PRKX and inhibits CREB-dependent transcriptional activation. *J Virol* 72(10):7916–7925.

27. Schultz DC, Friedman JR, Rauscher 3rd FJ (2001) Targeting histone deacetylase complexes via KRAB-zinc finger proteins: the PHD and bromodomains of KAP-1 form a cooperative unit that recruits a novel isoform of the Mi-2alpha subunit of NuRD. *Genes Dev* 15(4):428–443.

28. Schultz DC, Ayyanathan K, Negorev D, Maul GG, Rauscher 3rd FJ (2002) SETDB1: a novel KAP-1-associated histone H3, lysine 9-specific methyltransferase that contributes to HP1-mediated silencing of euchromatic genes by KRAB zinc-finger proteins. *Genes Dev* 16(8):919–932.

29. Ivanov A V., et al. (2007) PHD Domain-Mediated E3 Ligase Activity Directs Intramolecular Sumoylation of an Adjacent Bromodomain Required for Gene Silencing. *Mol Cell* 28(5):823–837.

30. Sripathy SP, Stevens J, Schultz DC (2006) The KAP1 corepressor functions to coordinate the assembly of de novo HP1-demarcated microenvironments of heterochromatin required for KRAB zinc finger protein-mediated transcriptional repression. *Mol Cell Biol* 26(22):8623–38.

31. Chang PC, et al. (2009) Kruppel-associated box domain-associated protein-1 as a latency regulator for Kaposi's sarcoma-associated herpesvirus and its modulation by the viral protein kinase. *Cancer Res* 69(14):5681–5689.

570 32. Rauwel B, et al. (2015) Release of human cytomegalovirus from latency by a
571 KAP1/TRIM28 phosphorylation switch. *Elife* 4(4). doi:10.7554/eLife.06068.
572 33. Rowe HM, et al. (2013) TRIM28 repression of retrotransposon-based enhancers is
573 necessary to preserve transcriptional dynamics in embryonic stem cells. *Genome Res*
574 23(3):452–461.
575 34. Wolf D, Goff SP (2007) TRIM28 mediates primer binding site-targeted silencing of murine
576 leukemia virus in embryonic cells. *Cell* 131(1):46–57.
577 35. Frietze S, O'Geen H, Blahnik KR, Jin VX, Farnham PJ (2010) ZNF274 recruits the histone
578 methyltransferase SETDB1 to the 39 ends of ZNF genes. *PLoS One* 5(12).
579 doi:10.1371/journal.pone.0015082.
580 36. Goodarzi AA, Kurka T, Jeggo PA (2011) KAP-1 phosphorylation regulates CHD3
581 nucleosome remodeling during the DNA double-strand break response. *Nat Struct Mol Biol*
582 18(7):831–839.
583 37. Li X, et al. (2007) Role for KAP1 serine 824 phosphorylation and
584 sumoylation/desumoylation switch in regulating KAP1-mediated transcriptional repression.
585 *J Biol Chem* 282(50):36177–36189.
586 38. Schwartz RA, et al. (2007) The Mre11/Rad50/Nbs1 complex limits adeno-associated virus
587 transduction and replication. *J Virol* 81(23):12936–12945.
588 39. Schmidt M, Afione S, Kotin RM (2000) Adeno-associated virus type 2 Rep78 induces
589 apoptosis through caspase activation independently of p53. *J Virol* 74(20):9441–9450.
590 40. Davis MD, Wu J, Owens R a (2000) Mutational analysis of adeno-associated virus type 2
591 Rep68 protein endonuclease activity on partially single-stranded substrates. *J Virol*
592 74(6):2936–2942.
593 41. Chejanovsky N, Carter BJ (1990) Mutation of a consensus purine nucleotide binding site in
594 the adeno-associated virus rep gene generates a dominant negative phenotype for DNA

595 replication. *J Virol* 64(4):1764–1770.
596 42. Li X, et al. (2010) SUMOylation of the transcriptional co-repressor KAP1 is regulated by
597 the serine and threonine phosphatase PP1. *Sci Signal* 3(119):ra32.
598 43. Pfeifer GP (2012) Protein phosphatase PP4: role in dephosphorylation of KAP1 and DNA
599 strand break repair. *Cell Cycle* 11(14):2590–2591.
600 44. Meiselbach H, Sticht H, Enz R (2006) Structural analysis of the protein phosphatase 1
601 docking motif: molecular description of binding specificities identifies interacting proteins.
602 *Chem Biol* 13(1):49–59.
603 45. Dutheil N, et al. (2014) Adeno-associated virus Rep represses the human integration site
604 promoter by two pathways that are similar to those required for the regulation of the viral
605 p5 promoter. *J Virol* 88(15):8227–8241.
606 46. Beullens M, et al. (2000) The C-terminus of NIPP1 (nuclear inhibitor of protein
607 phosphatase-1) contains a novel binding site for protein phosphatase-1 that is controlled by
608 tyrosine phosphorylation and RNA binding. *Biochem J* 352 Pt 3:651–658.
609 47. O'Connell N, et al. (2012) The molecular basis for substrate specificity of the nuclear
610 NIPP1:PP1 holoenzyme. *Structure* 20(10):1746–1756.
611 48. Verbinnen I, Ferreira M, Bollen M (2017) Biogenesis and activity regulation of protein
612 phosphatase 1. *Biochem Soc Trans* 45(September 2016):89–99.
613 49. Jagiello I, Beullens M, Stalmans W, Bollen M (1995) Subunit structure and regulation of
614 protein phosphatase-1 in rat liver nuclei. *J Biol Chem* 270(29):17257–63.
615 50. Jagiello I, et al. (1997) NIPP-1, a nuclear inhibitory subunit of protein phosphatase-1, has
616 RNA-binding properties. *J Biol Chem* 272(35):22067–71.
617 51. Bürck C, et al. (2015) KAP1 is a host restriction factor that promotes HAdV E1B-55K
618 SUMO modification. *J Virol* 90(2):JVI.01836-15.
619 52. Sun R, Liang D, Gao Y, Lan K (2014) Kaposi's sarcoma-associated herpesvirus-encoded

LANA interacts with host KAP1 to facilitate establishment of viral latency. *J Virol* 88(13):7331–7344.

53. Groner AC, et al. (2010) KRAB-zinc finger proteins and KAP1 can mediate long-range transcriptional repression through heterochromatin spreading. *PLoS Genet* 6(3):e1000869.

54. Zhang L, et al. (2014) Inhibition of KAP1 enhances hypoxia-induced Kaposi's sarcoma-associated herpesvirus reactivation through RBP-Jkappa. *J Virol* 88(12):6873–6884.

55. Schwartz RA, Carson CT, Schuberth C, Weitzman MD (2009) Adeno-associated virus replication induces a DNA damage response coordinated by DNA-dependent protein kinase. *J Virol* 83(12):6269–6278.

56. Collaco RF, Bevington JM, Bhrigu V, Kalman-Maltese V, Trempe JP (2009) Adeno-associated virus and adenovirus coinfection induces a cellular DNA damage and repair response via redundant phosphatidylinositol 3-like kinase pathways. *Virology* 392(1):24–33.

57. Seto E, Shi Y, Shenk T (1991) YY1 is an initiator sequence-binding protein that directs and activates transcription in vitro. *Nature* 354:241–245.

58. Nault J-C, et al. (2015) Recurrent AAV2-related insertional mutagenesis in human hepatocellular carcinomas. *Nat Genet* 47(10):1–15.

59. Zeltner N, Kohlbrenner E, Clement N, Weber T, Linden RM (2010) Near-perfect infectivity of wild-type AAV as benchmark for infectivity of recombinant AAV vectors. *Gene Ther* 17(7):872–879.

60. Morita E, Arii J, Christensen D, Votteler J, Sundquist WI (2012) Attenuated protein expression vectors for use in siRNA rescue experiments. *Biotechniques*:1–5.

61. Grimm D, Kern A, Rittner K, Kleinschmidt JA (1998) Novel tools for production and purification of recombinant adenoassociated virus vectors. *Hum Gene Ther* 9(18):2745–2760.

62. Hörer M, et al. (1995) Mutational analysis of adeno-associated virus Rep protein-mediated inhibition of heterologous and homologous promoters. *J Virol* 69(9):5485–96.

Figure Legends

Fig. 1. The latent AAV2 genome is repressed through KAP1 recruitment to the *rep* ORF and subsequent histone methylation. (*A-C*), AAV2 replication in control (shEMPTY) or KAP1-depleted (shKAP1) 293T cells. (*A*), Viral genome replication. (*B*), *Rep* and *cap* transcripts. Transcript levels represent fold changes over control cells infected with AAV2 + Ad5. Data are reported as mean±SEM, n=5. (*C*), AAV2 replication in KAP1-depleted cells complemented with exogenous KAP1. Data are reported as mean±SEM, n=4. (*D*), ChIP-qPCR performed on control or KAP1-depleted 293T cells infected with AAV2 (100 IU/cell) using anti-KAP1 antibody or IgG. Purified chromatin was analyzed by qPCR using primers for the viral p5 promoter or various regions of the *rep* and *cap* ORFs (right panel). *GAPDH* was used as a negative control, and the zinc finger genes *ZNF180* and *ZNF274* were used as positive controls (left panel). (*E*), ChIP-qPCR performed as described above, using anti-H3K9me3 antibody. Values represent fold enrichment over IgG. Values are reported as mean±SEM for 3 independent experiments. (*F-H*), AAV2 replication and protein expression in 293T cells depleted for CHD3 (siCHD3) and/or SETDB1 (siSETDB1). (*F*), AAV2 capsid (VP) protein expression and depletion of CHD3 and SETDB1 analyzed by western blotting. *(G)*, Quantification of VP3 levels using ImageJ software. (*H*), Viral genome replication analyzed by real time qPCR. Values are reported as mean±SEM, n=4. Statistical significance was determined by unpaired t test, $*P < 0.05$.

Fig. 2. Phosphorylation of KAP1-S824 is necessary for AAV2 transcription and replication. (*A*), p-KAP1-S824 in 293T cells infected with 10-10,000 gcp/cell of either AAV2 or rAAV2 in the presence of Ad5. (*B*), ChIP-qPCR performed as described for Fig. 1 D, E in 293T cells infected with AAV2

(100 IU/cell), with or without Ad5, n=1. (*C-D*), AAV2 genome replication in 293T cells overexpressing KAP1^{WT}, (*C*), or KAP1^{S824D}, (*D*). Values are reported as mean±SEM, n=4. (*E-F*), AAV2 replication in control cells and KAP1-depleted cells reconstituted with KAP1^{WT}, KAP1^{S824D}, KAP1^{S824A}, or treated with an empty vector control (EV). (*E*), Viral genome replication. Values are reported as mean±SEM, n=4. (*F*), AAV2 capsid (VP) and KAP1 protein levels. (*G*), AAV2 transcription in control cells and KAP1-depleted cells complemented with KAP1^{WT}, KAP1^{S824D}, or KAP1^{S824A}, or treated with an empty vector control (EV) 16h after infection with AAV2 (1 IU/cell) alone. Values are reported as mean±SEM, n=4. Statistical significance was determined by unpaired t test, **P* < 0.05, ***P* < 0.01, ****P* < .001.

Fig. 3. Rep52 and Rep78 mediate phosphorylation of KAP1-S824 through interactions with the protein phosphatase PP1. (*A*), p-KAP1-S824 in 293T cells infected with Ad5 alone, or coinfected with Ad5 and either AAV2 or rAAV2 (1,000 gcp/cell) monitored at 4, 18, 24, and 42 h post infection. (*B*), p-KAP1-S824 in 293T cells expressing the indicated Rep proteins. Values are reported as mean±SEM n=3. (*C*), GFP trap performed in 293T cells expressing Rep52 and GFP-tagged PP1 α, PP1 β, PP1 γ, or a GFP control. (*D-F*), AAV2 replication and transcription at different time points in 293T cells depleted for PP1 α (siPP1 α), PP1 β (siPP1 β), or both (siPP1 α/siPP1 β). (*D*), PP1 depletion analyzed by western blotting. (*E*), AAV2 genome replication. Values are reported as mean±SEM, n=7. (*F*), transcription from the three AAV2 promoters. Values are reported as mean±SEM, n=4. (*G*), Co-IP of FLAG-tagged proteins from 293T cells expressing FLAG-PP1 α or a FLAG-GFP control and the indicated Rep proteins. (*H*), Immunoblot of p-KAP1-S824 in 293T cells transfected with either Rep52, or Rep52^{K372A}. Protein levels were quantified using ImageJ software. Values are reported as mean±SEM n=3. Statistical significance was determined by unpaired t test, **P* < 0.05, ***P* < 0.01, ****P* < .001.

695 **Fig. 4.** Rep proteins interfere with NIPP1-PP1 complex to antagonize KAP1-S824
696 dephosphorylation. (*A*), Schematic representation of NIPP1 mutants. The N-terminal FHA domain is
697 shown in blue, and FHAm denotes the FHA binding mutant, which is unable to recruit
698 hyperphosphorylated proteins. The central PP1 binding domain containing the consensus PP1
699 binding site RVTF is shown in yellow. RATA denotes the PP1 binding mutant. The C-terminal PP1
700 interaction and inhibitory domain is shown in green, and the RNA binding region is shown in lime.
701 (*B*), Cross-linked GFP trap performed in cells expressing Rep52 and each of the GFP-tagged NIPP1
702 constructs, or a GFP control. (*C*), Immunoblot of p-KAP1-S824 in cells expressing NIPP1-WT, -
703 RATA, -FHAm or empty vector (EV) control. (*D*), Quantification of p-KAP1-S824 levels in C.
704 Values are reported as mean±SEM, n=4. (*E*), Immunoblot of p-KAP1-S824 in cells expressing Rep52
705 and NIPP1-WT, -RATA, -FHAm or an empty vector (EV) control (*F*), Quantification of p-KAP1-
706 S824 levels in e. Values are reported as mean±SEM, n=5. (*G*), Cross-linked GFP trap performed in
707 cells expressing NIPP1-WT-GFP and T7-tagged Rep52, $Rep52^{K372A}$ or a Renilla control. Statistical
708 significance was determined by unpaired t test, $*P < 0.05$.
709
710 **Fig. 5.** Model for release of AAV2 from KAP1-mediated latency. (*A*) Incoming AAV2 genomes
711 undergo second-strand synthesis, concatamerization, and chromatinization upon nuclear entry. KAP1
712 is recruited to the *rep* ORF via an unknown binding partner where it forms a scaffold for the
713 recruitment of SETDB1 and CHD3, leading to the methylation of AAV2-associated histones. NIPP1
714 is recruited to KAP1 via the FHA domain, where it serves to tether inactive PP1 to KAP1. (*B*), Upon
715 coinfection, KAP1 repression is partially lifted through several potential mechanisms – (1) helper-
716 mediated degradation of KAP1 as we have observed, (2) interference with KAP1 SUMOylation as
717 observed by others(51), and/or (3) phosphorylation of KAP1-S824 triggered by initial helper- or
718 AAV-mediated stress response – allowing for , (*C*), upregulation of *rep* by Ad5 E1A. Unknown
719 cellular factors/RNA binding inactivates NIPP1 allowing PP1 to restore baseline levels of p-KAP1-

720 S824. (*D*), Sequestration of PP1 by Rep sustains enhanced levels of phosphorylated KAP1-S824 to
721 support lytic replication.
722

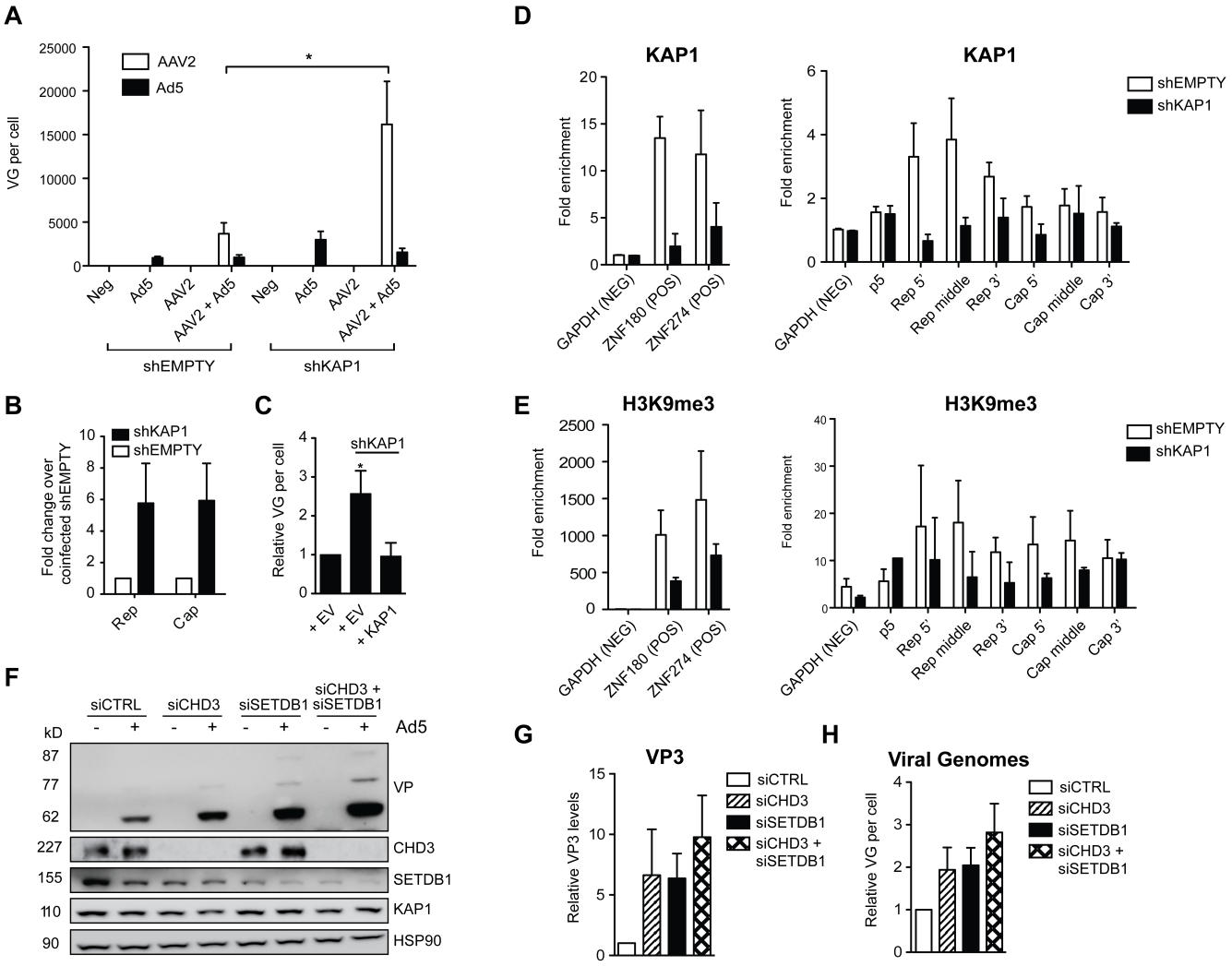
A
AAV2
Ad5
*
VG per cell
Neg
Ad5
AAV2
AAV2 + Ad5
shEMPTY
shKAP1
B
shKAP1
shEMPTY
Fold change over coinfected shEMPTY
Rep
Cap
C
shKAP1
Relative VG per cell
+ EV
+ EV
+ KAP1
D
KAP1
Fold enrichment
GAPDH (NEG)
ZNF180 (POS)
ZNF274 (POS)
shEMPTY
shKAP1
p5
Rep 5'
Rep middle
Rep 3'
Cap 5'
Cap middle
Cap 3'
E
H3K9me3
F
siCTRL
siCHD3
siSETDB1
siCHD3 + siSETDB1
Ad5
kD
87
77
62
227
155
110
90
VP
CHD3
SETDB1
KAP1
HSP90
G
VP3
Relative VP3 levels
H
Viral Genomes
Relative VG per cell

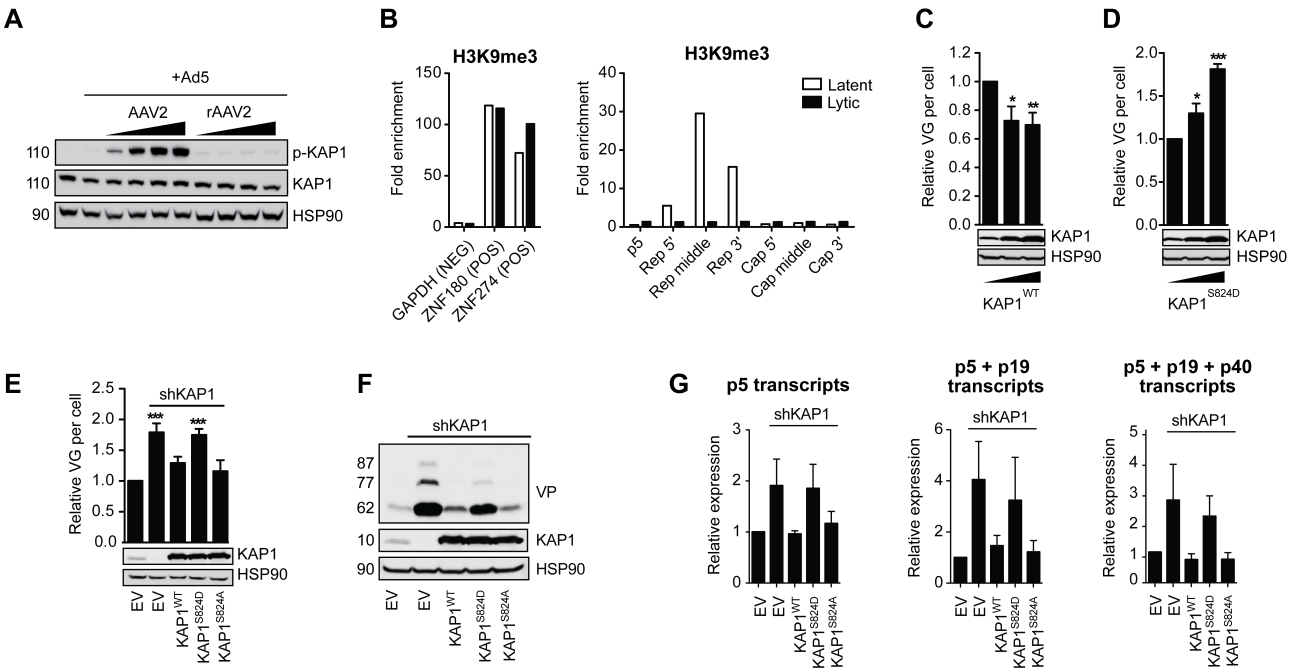
A
+Ad5
AAV2
rAAV2
110
p-KAP1
110
KAP1
90
HSP90
B
H3K9me3
Fold enrichment
GAPDH (NEG)
ZNF180 (POS)
ZNF274 (POS)
H3K9me3
Latent
Lytic
p5
Rep 5'
Rep middle
Rep 3'
Cap 5'
Cap middle
Cap 3'
C
Relative VG per cell
KAP1
HSP90
KAP1WT
D
Relative VG per cell
KAP1
HSP90
KAP1S824D
E
shKAP1
Relative VG per cell
KAP1
HSP90
EV
EV
KAP1WT
KAP1S824D
KAP1S824A
F
shKAP1
87
77
62
VP
10
KAP1
90
HSP90
EV
EV
KAP1WT
KAP1S824D
KAP1S824A
G
p5 transcripts
shKAP1
Relative expression
p5 + p19 transcripts
shKAP1
Relative expression
p5 + p19 + p40 transcripts
shKAP1
Relative expression

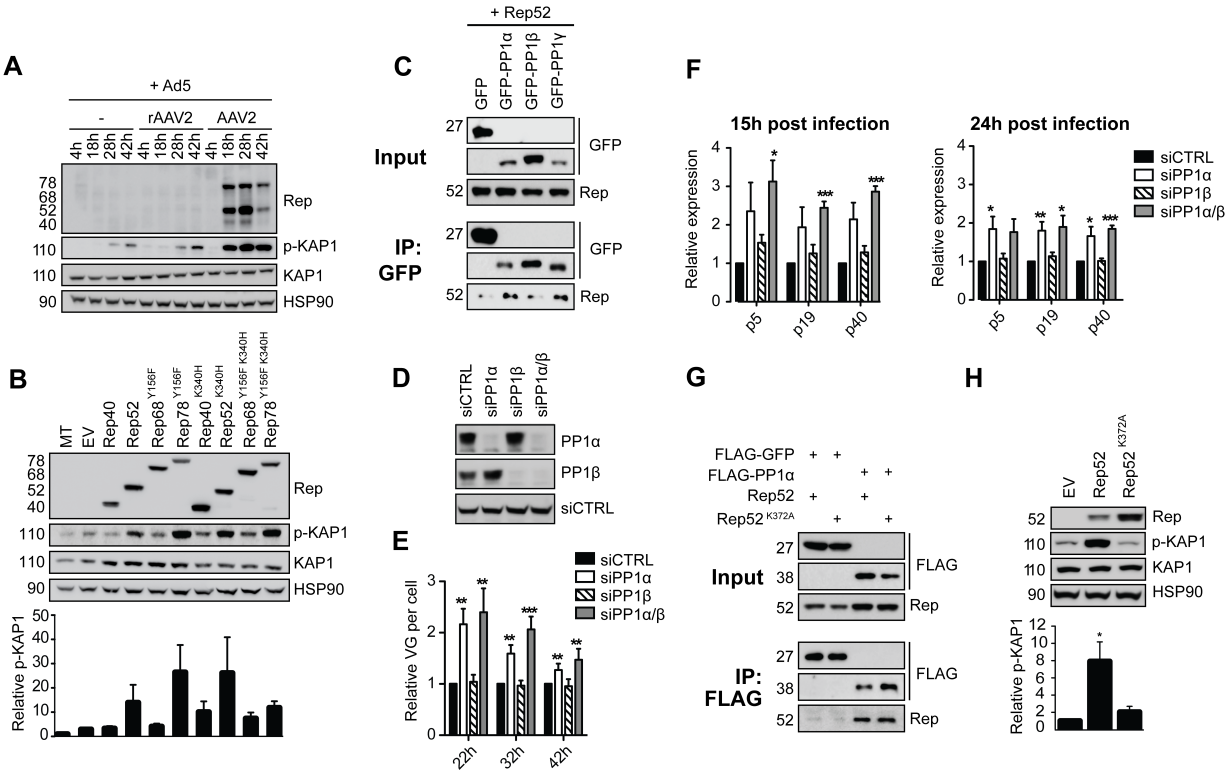
A
+ Ad5
-
rAAV2
AAV2
4h 18h 28h 42h 4h 18h 28h 42h 4h 18h 28h 42h
78
68
52
40
Rep
110
p-KAP1
110
KAP1
90
HSP90
B
MT
EV
Rep40
Rep52
Rep68 Y156F
Rep78 Y156F
Rep40 K340H
Rep52 K340H
Rep68 Y156F K340H
Rep78 Y156F K340H
Rep
p-KAP1
KAP1
HSP90
Relative p-KAP1
C
+ Rep52
GFP
GFP-PP1α
GFP-PP1β
GFP-PP1γ
Input
IP: GFP
27
52
GFP
Rep
D
siCTRL
siPP1α
siPP1β
siPP1α/β
PP1α
PP1β
siCTRL
E
siCTRL
siPP1α
siPP1β
siPP1α/β
Relative VG per cell
22h
32h
42h
F
15h post infection
24h post infection
Relative expression
siCTRL
siPP1α
siPP1β
siPP1α/β
p5
p19
p40
G
FLAG-GFP
FLAG-PP1α
Rep52
Rep52 K372A
Input
IP: FLAG
27
38
52
FLAG
Rep
H
EV
Rep52
Rep52 K372A
Rep
p-KAP1
KAP1
HSP90
Relative p-KAP1

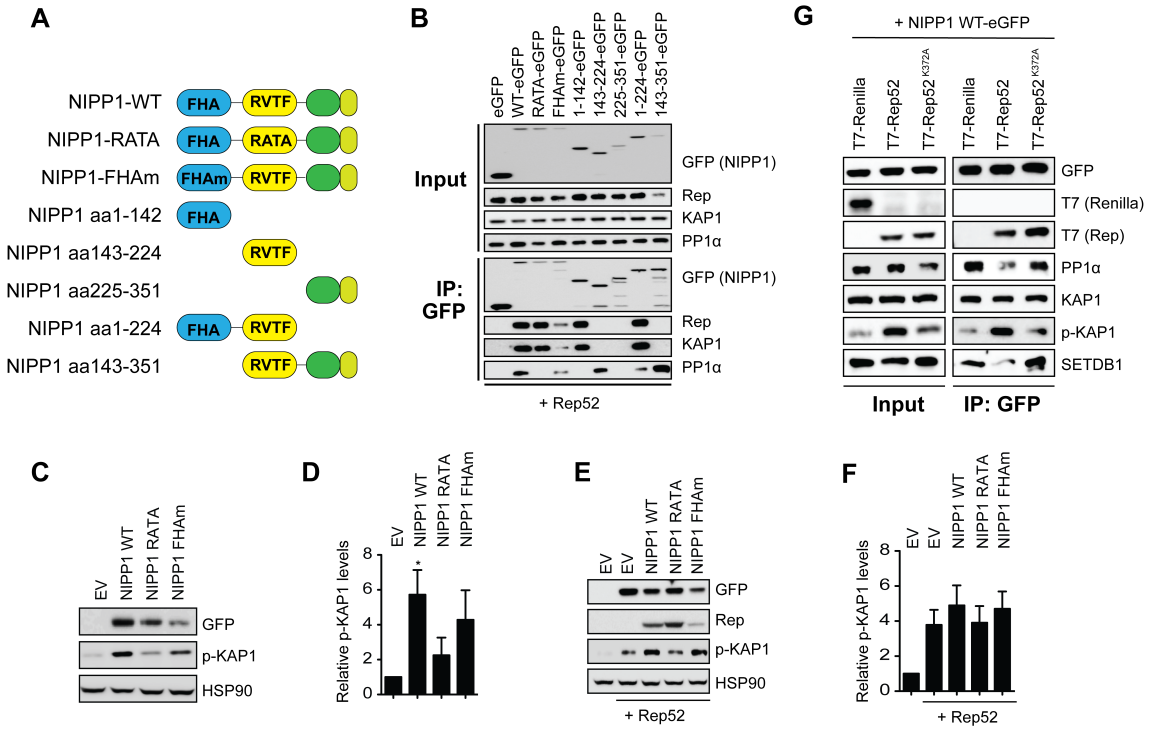
A
NIPP1-WT
NIPP1-RATA
NIPP1-FHAm
NIPP1 aa1-142
NIPP1 aa143-224
NIPP1 aa225-351
NIPP1 aa1-224
NIPP1 aa143-351
FHA
RVTF
RATA
FHAm
B
eGFP
WT-eGFP
RATA-eGFP
FHAm-eGFP
1-142-eGFP
143-224-eGFP
225-351-eGFP
1-224-eGFP
143-351-eGFP
Input
IP: GFP
GFP (NIPP1)
Rep
KAP1
PP1α
+ Rep52
G
+ NIPP1 WT-eGFP
T7-Renilla
T7-Rep52
T7-Rep52 K372A
GFP
T7 (Renilla)
T7 (Rep)
PP1α
KAP1
p-KAP1
SETDB1
Input
IP: GFP
C
EV
NIPP1 WT
NIPP1 RATA
NIPP1 FHAm
GFP
p-KAP1
HSP90
D
Relative p-KAP1 levels
0
2
4
6
8
*
E
Rep
+ Rep52
F

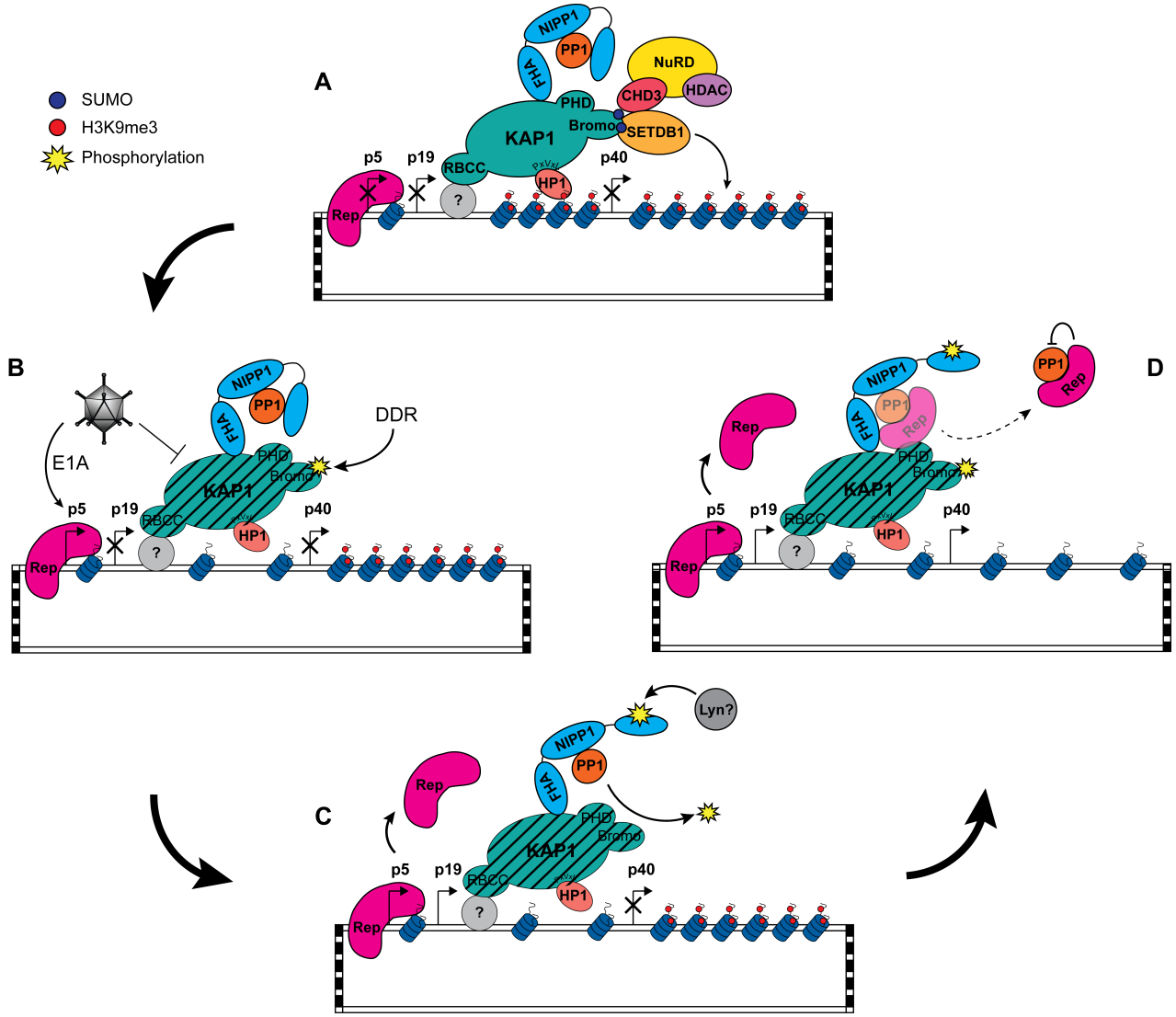
SUMO
H3K9me3
Phosphorylation
A
NIPP1
PP1
FHA
NuRD
CHD3
HDAC
PHD
Bromo
KAP1
SETDB1
p5
p19
RBCC
p40
HP1
?
Rep
B
E1A
DDR
C
Lyn?
D

Supporting Information

SI Materials and Methods

Plasmids

pcDNA-mycBirAR118G, pCMV-Rep40 (pND229), pCMV-Rep52 (pND230), pCMV-Rep68 Y156F M225G (pND226), and pCMV-Rep78 Y156F M225G (pND227) have been previously described (45). BirA* and each of the Rep sequences were amplified by PCR, after which overlapping PCR was used to fuse the BirA* fragment to the N-terminus of each Rep fragment. The resulting amplicons were cloned into pcDNA3.1+. FLAG- and T7-tagged Rep proteins were generated by cloning of Rep PCR products into either the pEGFP-C1 vector (Clontech) containing N-terminal FLAG tag or T7 tag, respectively. K372A mutants were generated by site-directed mutagenesis. ZNF truncation mutants were generated by PCR amplification of aa 1-529 (Δ91/87), 1-558 (Δ63), or 1-577 (Δ44), using either pND230 or pND227 as a template. The amplified fragments were then cloned into the N-terminal T7 vector described above. FLAG-PP1α was generated by cloning of PCR-amplified PP1α from an EST clone obtained from Genome Cube (Clone IRAUp969F0817D) into the N-terminal FLAG-vector described above. pC1-FLAG-wtKAP1 was provided by Helen Rowe and was used for cloning of PCR-amplified wtKAP1 into untagged pcDNA3.1+. PP1γ-NIPP1, and NIPP1-WT, -RATA, -FHAm, -aa1-142, -aa143-224, -aa225-251, -aa1-224, and -aa143-351 fused to eGFP were provided by Mathieu Bollen.

Western Blot Analysis

Cells were lysed in RIPA buffer, and proteins were separated on a 6-12% SDS-PAGE gel and transferred to a nitrocellulose membrane (Hybond-C Extra nitrocellulose, Amersham Biosciences). Membranes were blocked with either 5% nonfat dry milk or 2.5% BSA (for phospho-antibodies) in PBS containing 0.5% Tween-20 (PBST) for 45 minutes at RT and then incubated with primary antibody for 2h at room temperature. The membranes were then washed 3x10’ in PBST and incubated

with HRP-conjugated anti-mouse or anti-rabbit IgG (BioRad) for 1h at RT. After 3x10' washes in PBST, membranes were developed using West Pico ECL reagent (Thermo Scientific). The following primary antibodies were used**:** HSP90 (Santa Cruz, sc-69703; 1:10,000), KAP1 (Chemicon, MAB3662; 1:000), p-KAP1-S824 (Bethyl, A300-767A; 1:2000), VP (ARP, 03-61058; 1:500), Rep (Progen, 61069; 1:100), dsRed (Clontech, 632496; 1:2000), CHD3 (Bethyl, A301-219A; 1:4000), SETDB1 (Abcam, ab12317; 1:1000), FLAG (Sigma, F1804; 1:1000), T7 (Merck Millipore, 69522-3; 1:10,000), pChk2 (NEB, 2661S; 1:1000), GFP (Roche, 11814460001; 1:5000), PP1α (Cambridge Bioscience, A300-904A; 1:1000), PP1β (Cambridge Bioscience, A300-905A; 1:1000), PP1γ (Santa Cruz, sc-6108; 1:1000), and avidin peroxidase (Sigma; 1:8000).

Lentiviral transductions

pC-SIREN-based lentiviral vectors expressing either a hairpin targeting the 3'UTR of KAP1 (shKAP1; GATCCGCCTGGCTCTGTTCTCTGTCCTTTCAAGAGAAGGA CAGAGAACAGAG CCAGGTTTTTTACGCGTG) or the corresponding empty vector (shEMPTY) were provided by Helen Rowe. pCSIG-eGFP lentiviral vectors provided by Stuart Neil were modified to contain the truncated CMVΔ5 promoter (60) in place of the SFFV promoter, and to express KAP1-WT, KAP1-S824D, or KAP1-S824A. Lentiviral vector-containing supernatants were produced by the common triple transfection method using the VSV-G plasmid, HIV-Gag/Pol/Rev/Tat packaging plasmid, and the lentiviral transfer plasmid in a 3:2:1 molar ratio. Supernatants were harvested 48 and 72 hours after transfection, pooled, filtered, and frozen at -80^{o}C until use. For transduction, 1 x 10^{6} 293T cells were transduced in a 6-well format using 0.5-1.6 mL of particle-containing supernatant diluted with the appropriate amount of DMEM + 10% FBS. For complementation experiments, cells were transduced with pCSIG-based expression constructs and either shKAP1 or shEMPTY 72h later. Cells were then infected with AAV and Ad5 48h after knockdown.

Immunofluorescence

293T cells were seeded at a density of $2x10^5$/mL on poly-L-lysine (Sigma) coated coverslips in 24-well plates the day prior to transfection. 4h prior to transfection, DMSO or ATMi was added to the appropriate wells to a final concentration of 10μM. Cells were then transfected with 20ng of empty vector or pRep78-GFP using 2μl Lipofectamine 2000 in 50μl serum-free Opti-mem. The next day, cells were infected with Ad5 (2 PFU/cell) in a total volume of 160μl for 1 h, after which the medium was replaced with fresh DMEM + 10% FBS. Cells were fixed 24h after Ad5 infection in 4% PFA for 10' at room temperature, washed in PBS, permeabilized in 0.1% Triton-X-100 for 10' at room temperature, and washed again in PBS. Cells were then incubated with primary antibody (α-p-KAP1-S824 antibody; 1:1000) diluted in PBS + 1% BSA for 2h at room temperature, washed, and then incubated with secondary antibody (Biolegend; rabbit IgG2b-AlexaFluor 594, 1 μg/ml (1:1000) diluted in PBS for 1h at room temperature. Cells were then washed a final time and mounted in Prolong Gold Antifade Reagent (Invitrogen). Images were visualized using an Eclipse Ti-E Inverted confocal microscope and analyzed with NIS Elements C software.

siRNA transfections. In a 24-well format, 2 x 10^5 cells were transfected with 50nM (siKAP1.2 [GAAAUGUGAGCGUGUACUG] and siKAP1.4 [GAACGAGGCCUUCG GUGAC]) or 100nM (siCHD3 [Dharmacon, L-005046-00-0005] and siSETDB1 [Dharmacon, L-020070-00-0005]) siRNA using 2ul Dharmafect (Dharmacon) in 50ul Optim-mem (Gibco). 6h later, medium was replaced with fresh DMEM + 10% FBS. 24h after transfection, cells were re-plated into 12-well format. 36h after transfection, cells were subjected to a second transfection as described above, using 4ul Dharmafect in 100ul Opti-mem. 4h after the second transfection, cells were infected with 10 IU/cell AAV2 and 2 PFU/cell of Ad5 as described for the viral replication experiments. For PP1 depletion experiments, cells were transfected only once with a total of 40nM siPP1α (Dharmacon, L-

008927-00-0005), siPP1β (Dharmacon, L-008685-00-0005), or both as described above. 24h after transfection, cells were re-plated into a 12-well format for infection the next day as described above.

Real-time PCR

For analysis of viral replication, total DNA was extracted using the Qiagen DNeasy Blood and Tissue DNA extraction kit. Viral DNA was quantified by real-time PCR using the SYBR Green JumpStart Taq ReadyMix for qPCR (Sigma-Aldrich) using an ABI PRISM system (Applied Biosystems). Cap and Ad5 100kd-specific primers and a pDG-based (61) standard curve were used for absolute quantification; the signal was normalised to cyclophilin. Primers: Cap FW (5' – TTCTCAGATGCTGC GTACCGGAAA – 3'), Cap RV (5' – TCTGCCATTGAGGTGGTACTTGGT – 3'), Ad5 100kd FW (5'-TCATTACCCAGGGCCACATT – 3'), Ad5 100kd RV (5' – CCTCGTCCAAAACCTCCTCT – 3'), cyclophilin FW (5' – TGCTGGACCCAAC ACAAATG – 3'), cyclophilin RV (5' – TGCCATCCAACCACTCAGTCT – 3').

qRT-PCR

Total RNA was extracted using the RNeasy kit (Qiagen) after DNAseI (Qiagen) treatment for 15 minutes at 37˚C. Reverse transcription was performed using the High Capacity Reverse Transcription kit (Applied Biosystems). cDNA was quantified by real-time qPCR on an ABI PRISM system (Applied Biosystems) using the TaqMan Universal PCR master mix (Life Technologies and custom designed primer-probe mixes (Eurofins). Primers: p5 FW (5'- AACAAGGTGGTGGATGAGT - 3'), p5 RV (5' – CGTTTACGCTCCGTGAGATT - 3'), p40 FW (5' – GGAAGCAAGGCTCAGAGAAA -3') and p40 RV (5' – CCTCTCTGGAGGTTGG TAGATA - 3'). Probes: p5 (5' - FAM-ACGTGGTTGAGGTGGAGCATGAT-TAM - 3'), and p40 (5' - FAM-AGGAAATCAGGACAA CCAATCCCGT-TAM - 3'). Relative expression levels were determined

with the ΔΔCt quantification method using 18s ribosomal RNA (Taqman Pre-developed assay reagents, human 18S rRNA, Applied Biosystems) as a housekeeping reference gene.

Analysis of p-KAP1-S824 levels

Phosphorylation of KAP1-S824 was investigated in 293T cells that were either infected with AAV2/Ad5 or transfected with various Rep-expressing constructs using linear PEI or NIPP1-expressing constructs using TransIT-LT1 (Mirus). Where relevant, cells were pretreated with either DMSO or 10μM ATMi 4h prior to infection/transfection, and inhibitors were maintained throughout. Infections were performed as described above, and transfections were performed at ~70% confluency using 1μg DNA/8x10^5 cells and 4μl PEI/μg DNA. Medium was changed 6h after transfection, and cells were harvested for western blot 27h after infection/transfection.

SI Figure Legends

Fig. S1. The AAV2 Rep Proteins Physically Interact with KAP1. (*A*) Immunoblot of biotinylated proteins purified from BirA*-Rep52 BioID screen using anti-KAP1. (*B*), Verification of BioID using exogenous FLAG-KAP1; purified biotinylated proteins from 293T cells expressing FLAG-KAP1 with either empty vector (EV) or BirA*-Rep52 were analyzed for Rep and KAP1 by western blot. (*C*), Cross-linked co-IP for FLAG-tagged proteins from 293T cells expressing FLAG-KAP1 or a FLAG-GFP control and each of the four Rep proteins. (*D*), Cross-linked co-IP for FLAG-tagged proteins from lysates of 293T cells expressing FLAG-GFP, FLAG-Rep40, FLAG-Rep52, FLAG-Rep68, or FLAG-Rep78 and KAP1 from transfected 293T cells.

Fig. S2. AAV2 replication and protein expression in KAP1-depleted cells. (*A*) Rep and capsid protein (VP) expression, and KAP1 knockdown efficiency in AAV2 and Ad5 infected control (shEMPTY) and KAP1-depleted (shKAP1) 293T cells. Data are reported as mean±SEM, n=3. (*B*), AAV2 replication in control (siCTRL) or KAP1-depleted (siKAP1.2/siKAP1.4) cells. Viral genome replication was analyzed by qPCR, and KAP1 knockdown efficiency was analyzed by western blot. Data are reported as mean±SEM, n=4. (*C*), AAV2 capsid (VP) and KAP1 protein levels at different time points in control cells and KAP1-depleted cells complemented with shRNA-resistant *KAP1* or an empty vector control (EV) and coinfected with AAV2 and Ad5.

Fig. S3. ChIP-qPCR performed on control or KAP1-depleted 293T cells infected with AAV2 (100 IU/cell). Purified chromatin was analyzed by qPCR using primers for the viral p5 promoter or various regions of the *rep* and *cap* ORFs. *GAPDH* was used as a negative control, and the zinc finger genes *ZNF180* and *ZNF274* were used as positive controls. Each of the three independent repeats are shown for (*A*) KAP1-specific and (*B*) H3K9me3-specific ChIP experiments (Fig. 1 *D* and *E*).

Fig. S4. Phosphorylation of KAP1-S824 by the Rep proteins is independent from ATM activation. (*A*), p-KAP1-S824 localization in 293T cells pretreated with ATMi and expressing Rep78-GFP with and without Ad5 infection (left and right panel, respectively). (*B-C*), p-KAP1-S824 levels analyzed in 293T cells pretreated with ATMi. (*B*), Cells were transfected with EV, Rep52, or Rep78. p-Chk2 was monitored to assess efficiency of ATM inhibition. p-KAP-S824 levels were normalized to Rep levels to correct for differences in transfection efficiency as a result of pretreatment with ATMi. (*C*), Cells were infected with AAV2 and Ad5. Values are reported as mean±SEM, n=4.

Fig. S5. Phosphorylation of KAP1-S824 in the presence of Rep52 and Rep78 is dependent on the Rep C-terminal zinc finger domain. (*A*), Schematic diagram representing full length Rep52, comprising an ATPase domain (AAA+) and zinc finger domain (ZNF), and the C-terminal truncation mutants in which the ZNF domain is progressively removed. Black bars indicated a CXXC zinc-binding motif, and red bars a CXXH zinc-binding motif. (*B*), p-KAP1-S824 in 293T cells transfected with full length Rep52 and Rep78, or truncation mutants in which the C-terminal ZNF domain is progressively removed. Values are reported as mean±SEM, n=3. (*C*), Cross-linked co-IP for FLAG-tagged proteins from 293T cells expressing FLAG-KAP1, or a FLAG-GFP control, with full length Rep52 or each of the Rep52 C-terminal ZNF truncation mutants. Statistical significance was determined by unpaired t test, $*P < 0.05$, $**P < 0.01$, $***P < .001$.

Fig. S6. Validation of Rep-K372A PP1-binding mutant. (*A*), Depiction of the PP1-binding site in the Rep ATPase domain. The Walker B motif is outlined in black, and the partially overlapping consensus binding site is outlined in pink. Lysine 372 alone was subjected to mutagenesis in order to preserve Rep ATPase/helicase function. (*B*), Rep-mediated repression of AAV2 p5 is dependent on a functional ATPase/helicase domain (62). To verify ATPase activity of $Rep52^{K372A}$, 293T cells co-transfected with a p5-mCherry reporter construct and Rep52 or $Rep52^{K372A}$ expression plasmids were

analyzed for p5 activity by western blotting for mCherry (45). Protein levels were quantified using Image J software. Values are reported as mean±SEM, n=3. (*C*), Cross-linked co-IP for FLAG-tagged proteins from 293T cells expressing FLAG-KAP1, or a FLAG-GFP control, with the various Rep proteins.

Fig. S7. Ad5 and HSV-1 infection leads to KAP1 degradation. (*A-B*), Immunoblot of KAP1 in 293T cells (*A*) and HeLa cells (*B*) infected with Ad5 at the stated MOI (PFU/cell). Values are reported as mean±SEM, n=3. (*C*), Immunoblot of KAP1 in HeLa cells treated with MG132 at the stated concentrations and infected with 10 PFU/cell of Ad5. (*D-E*), Immunoblot of endogenous KAP1 in 293T, (*D*), and HeLa, (*E*), cells infected with HSV-1. Values are reported as mean±SEM, n=3. Statistical significance was determined by unpaired t test, $*P < 0.05$, $**P < 0.01$, $***P < .001$.

Fig. S8. Model for regulation of KAP1-S824 phosphorylation by NIPP1, PP1, and Rep. Schematic representation of a model for the regulation of KAP1-S824 phosphorylation by NIPP1, PP1, and Rep. The upper series represents regulation in the absence of AAV2 infection. Inactive NIPP1-PP1 is recruited to KAP1 via the NIPP1 FHA domain. Initiation of a DNA damage response (DDR) leads to phosphorylation of KAP1-S824, allowing for heterochromatin relaxation and repair. The DDR also leads to the inactivation of NIPP1 through phosphorylation of the C-terminal region, possibly through the tyrosine kinase Lyn, allowing PP1 to restore homeostatic levels of p-KAP1-S824. In the event of AAV2/Ad5 coinfection however, Rep interferes with this pathway by competing for PP1 and thus acts to maintain high levels of p-KAP1-S824 triggered by infection.

SI Table 1. Peptides identified by BioID for KAP1 and various known interaction partners of the Rep proteins.

Identified Protein	Accession Number	Bait Protein	Unique Peptides	Sequence Coverage	Protein ID Probability
KAP1	Q13263	BirA*-Rep40	2	3.1%	100%
		BirA*-Rep52	8	12.9%	100%
		BirA*-Rep68	3	6.0%	100%
		BirA*-Rep78	1	1.3%	100%
RUVBL1	Q9Y265	BirA*-Rep40	2	7.2%	100%
		BirA*-Rep52	7	22.1%	100%
		BirA*-Rep68	1	2.9%	99%
		BirA*-Rep78	1	2.9%	99%
MRE11	P49959	BirA*-Rep40	1	2.0%	99%
		BirA*-Rep52	8	19%	100%
SNW1	Q5R7R9	BirA*-Rep40	5	23.7%	100%
		BirA*-Rep52	9	24.1%	100%
		BirA*-Rep68	1	2.8%	100%
		BirA*-Rep78	2	4.3%	100%
MDC1	Q14676	BirA*-Rep40	2	2.0%	100%
		BirA*-Rep52	4	3.3%	100%
		BirA*-Rep68	1	0.5%	100%

TAF1/SET	Q01105	BirA*-Rep40	1	4.8%	100%
		BirA*-Rep68	1	4.8%	100%
NUCLEOLIN	P19338	BirA*-Rep40	1	2%	99%
		BirA*-Rep52	10	16.2%	100%
		BirA*-Rep68	13	18%	100%
		BirA*-Rep78	4	6.2%	100%

SI Table 2. ChIP-qPCR primers

Gene	**FW**	**RV**
GAPDH	CACCGTCAAGGCTGAGAACG	ATACCCAAGGGAGCCACACC
ZNF180	TGATGCACAATAAGTCGAGCA	TGCAGTCAATGTGGGAAGTC
ZNF274	GGAGAAATCCCATGAGGGTAA	GGCTTTTGTGAGAATGTTTTCC
p5	CTGTATTAGAGGTCACGTGAGTG	TCAAACCTCCCGCTTCAAA
Rep 5’	CCGAGAAGGAATGGGAGTT	CCATTCCGTCAGAAAGTCG
Rep middle	GCCTTGGACAATGCGGGAAAGATT	TGTCGACACAGTCGTTGAAGGGAA
Rep 3’	TTCCCGTGTCAGAATCTCAA	CCAAATCCACATTGACCAGA
Cap 5’	GACAGTGGTGGAAGCTCAAA	TTGTACCCAGGAAGCACAAG
Cap middle	TTCTCAGATGCTGCGTACCGGAAA	TCTGCCATTGAGGTGGTACTTGGT
Cap 3’	GTCAGCGTGGAGATCGAGT	AGGCTCTGAATACACGCCAT

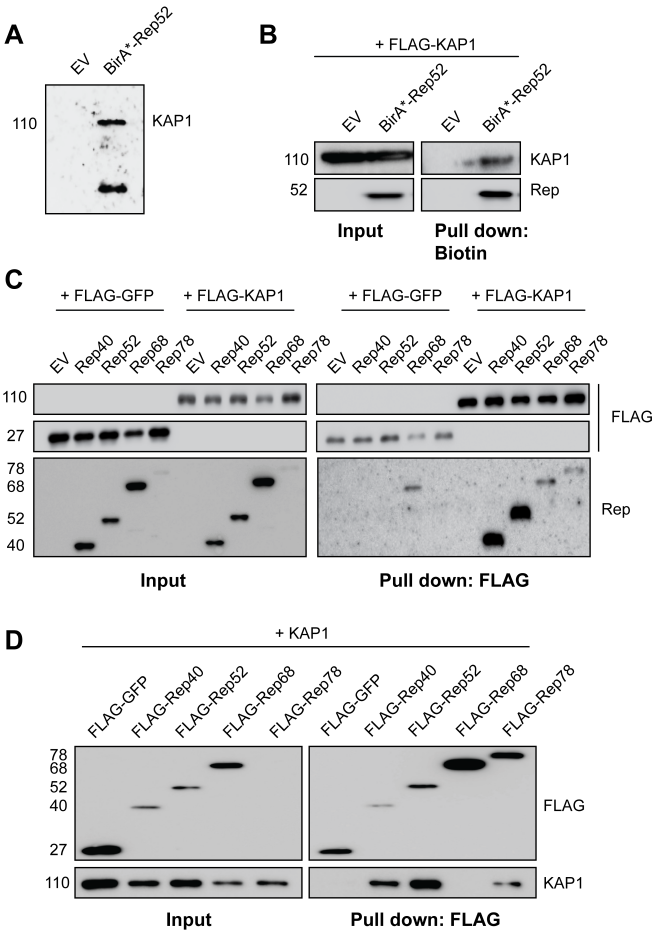
A
EV
BirA*-Rep52
110
KAP1
B
+ FLAG-KAP1
EV
BirA*-Rep52
EV
BirA*-Rep52
110
52
KAP1
Rep
Input
Pull down:
Biotin
C
+ FLAG-GFP
+ FLAG-KAP1
+ FLAG-GFP
+ FLAG-KAP1
EV
Rep40
Rep52
Rep68
Rep78
110
27
78
68
52
40
FLAG
Rep
Input
Pull down: FLAG
D
+ KAP1
FLAG-GFP
FLAG-Rep40
FLAG-Rep52
FLAG-Rep68
FLAG-Rep78
78
68
52
40
27
110
FLAG
KAP1
Input
Pull down: FLAG

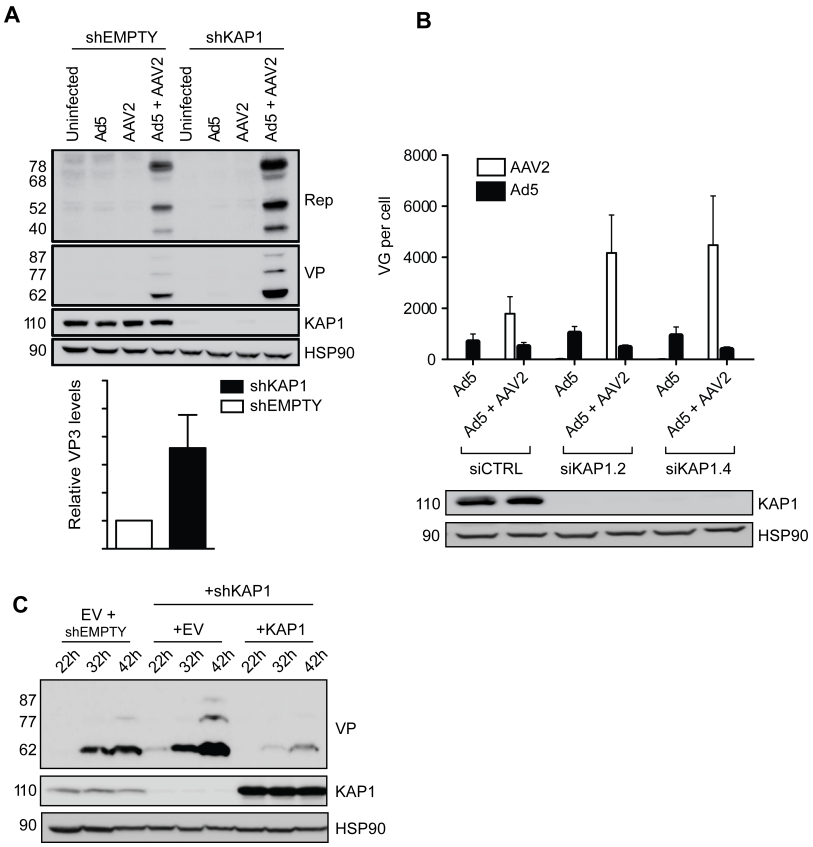
A
shEMPTY
shKAP1
Uninfected
Ad5
AAV2
Ad5 + AAV2
78
68
52
40
Rep
87
77
62
VP
110
KAP1
90
HSP90
Relative VP3 levels
shKAP1
shEMPTY
B
AAV2
Ad5
VG per cell
8000
6000
4000
2000
0
Ad5
Ad5 + AAV2
siCTRL
siKAP1.2
siKAP1.4
110
KAP1
90
HSP90
C
+shKAP1
EV + shEMPTY
+EV
+KAP1
22h
32h
42h
87
77
62
VP
110
KAP1
90
HSP90

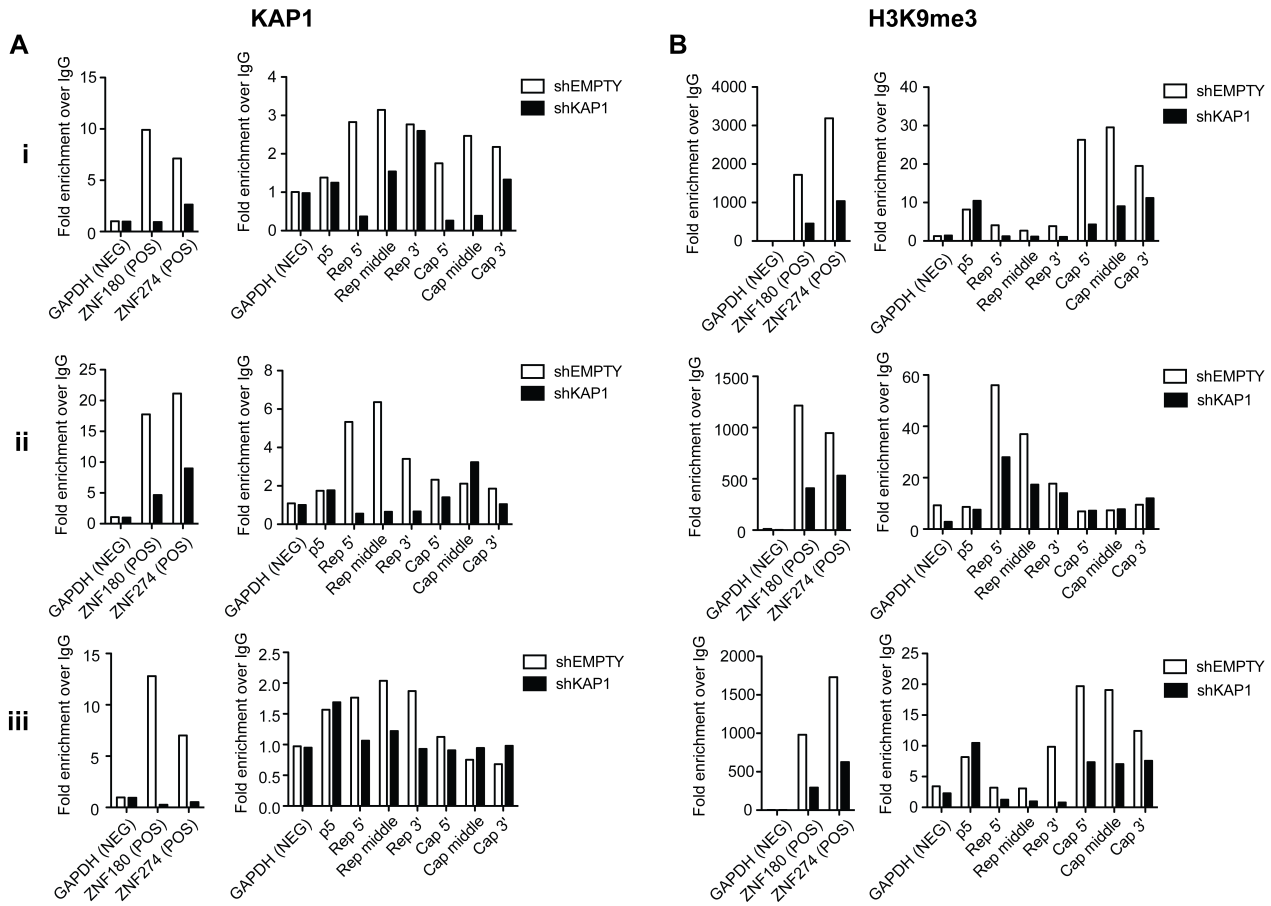
A
KAP1
B
H3K9me3
i
ii
iii
Fold enrichment over IgG
shEMPTY
shKAP1
GAPDH (NEG)
ZNF180 (POS)
ZNF274 (POS)
p5
Rep 5'
Rep middle
Rep 3'
Cap 5'
Cap middle
Cap 3'

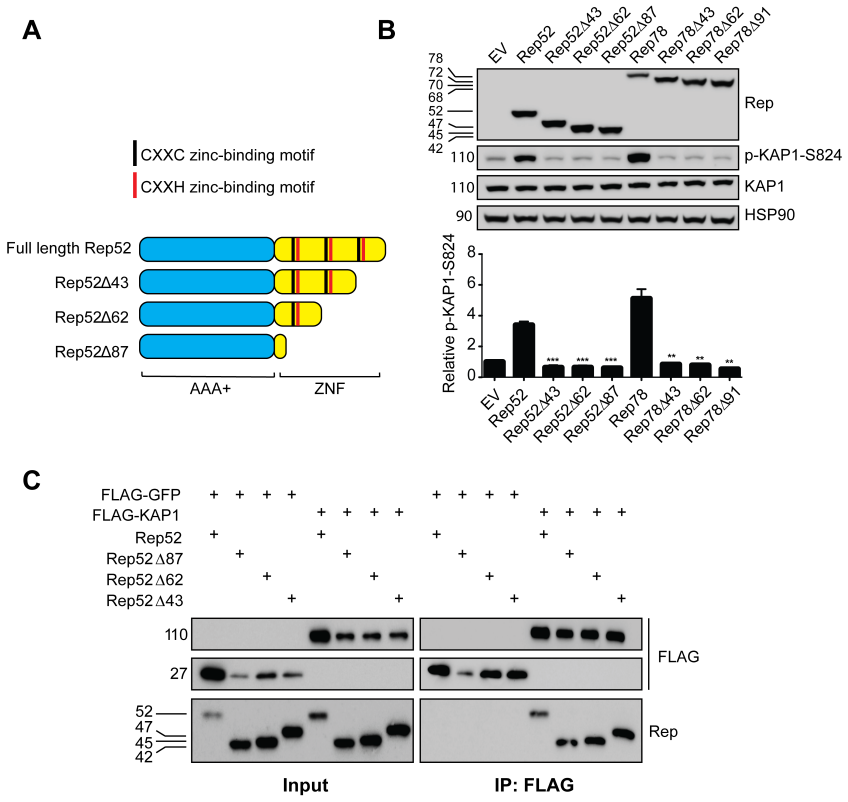
A
CXXC zinc-binding motif
CXXH zinc-binding motif
Full length Rep52
Rep52Δ43
Rep52Δ62
Rep52Δ87
AAA+
ZNF
B
EV
Rep52
Rep52Δ43
Rep52Δ62
Rep52Δ87
Rep78
Rep78Δ43
Rep78Δ62
Rep78Δ91
78
72
70
68
52
47
45
42
Rep
110
p-KAP1-S824
110
KAP1
90
HSP90
Relative p-KAP1-S824
8
6
4
2
0
***
**
C
FLAG-GFP
FLAG-KAP1
Rep52
Rep52Δ87
Rep52Δ62
Rep52Δ43
110
27
FLAG
52
47
45
42
Rep
Input
IP: FLAG

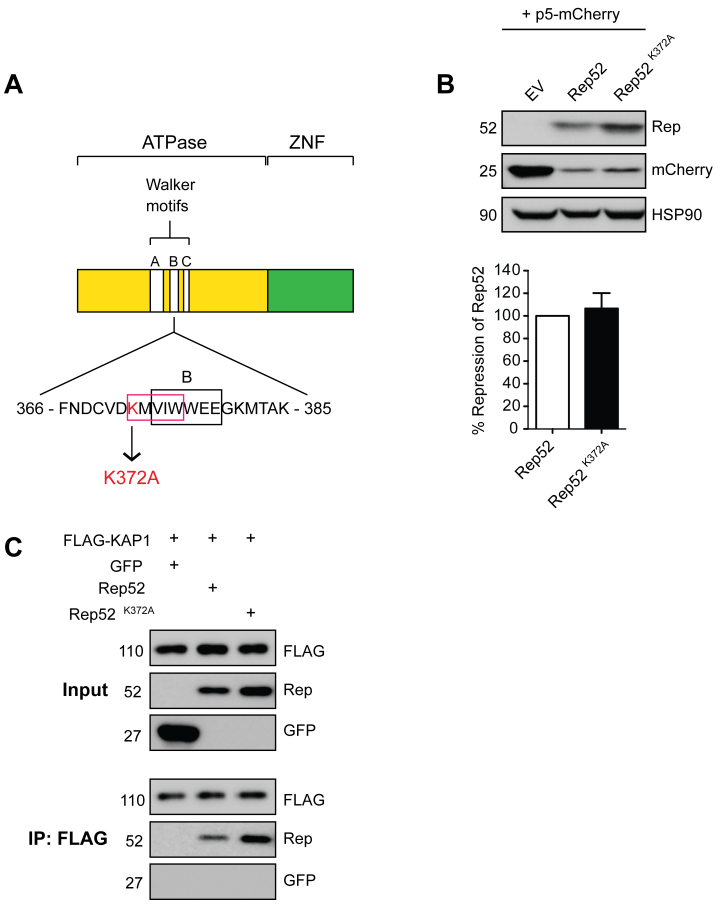
A
ATPase
ZNF
Walker
motifs
A B C
B
366 - FNDCVDKMVIWWEEGKMTAK - 385
K372A
B
+ p5-mCherry
EV
Rep52
Rep52 K372A
52
Rep
25
mCherry
90
HSP90
% Repression of Rep52
140
120
100
80
60
40
20
0
Rep52
Rep52 K372A
C
FLAG-KAP1 + + +
GFP +
Rep52 +
Rep52 K372A +
110
FLAG
Input
52
Rep
27
GFP
110
FLAG
IP: FLAG
52
Rep
27
GFP